LUNDS UNIVERSITET

KBTM01 Master's Degree Project in Biotechnology, 30 credits

Cloning and expressing the genes encoding Glycerol dehydratase (GDHt) and 1,3-Propanediol dehydrogenase (1,3-PDDH) in *E. coli*

Pechlivani Eleni
Student number: 19970419-8341

Conducted at Division of Biotechnology,
Faculty of Engineering, LTH
Department of Chemistry, Lund University

Supervisor: Dr. Mohamed Ismail
Examiner: Prof. Rajni Hatti-Kaul

Acknowledgments

To begin with, I would like to express my gratitude towards Prof. Rajni Hatti-Kaul for introducing me to the project and providing me with the opportunity to collaborate with her research team. It was an honor to be a part of this research endeavor, and I learned a great deal from the experience. Furthermore, I would like to extend my gratitude towards my supervisor, Dr. Mohamed Ismail, and co-supervisors Dr. Nélida Leiva Eriksson and Dr. Mahmoud Sayed Ali Sayed, for their unwavering guidance and support throughout the project. They provided valuable insights, helped me to navigate challenging aspects of the research, and enabled me to develop a better understanding of the research process. Moreover, I would like to extend my thanks to all members of the Biotechnology division for their technical support, advice, and for creating a positive work environment. Working alongside them was a pleasure, and I am grateful for this valuable experience.

My final thank you goes to my family and friends, who have been a constant source of support and encouragement throughout this journey. I want to thank my parents for always believing in me, even during moments when I struggled to believe in myself. To my friends, I am immensely grateful for the laughter, companionship, and cherished memories that we have shared during this experience, and which I will treasure for a lifetime.

Table of Contents

Abbreviations

Abbreviation	Meaning
1,3-PDDH	1,3-propanediol dehydrogenase
1,3-PDO	1,3-propanediol
3-HP	3-hydroxypropionic acid
3-HPA	3-hydroxypropionaldehyde
ALDH	Aldehyde dehydrogenase
B12	Vitamin B12, Cob(II)alamin
coB12	5′-deoxyadenosylcobalamin
DHA	Dihydroxyacetone
DHAK	Dihydroxyacetone kinase
EDTA	Ethylenediaminetetraacetic acid
GDH	Glycerol dehydrogenase
GDHt	Glycerol dehydratase
GDHtR	Glycerol dehydratase reactivase
GLPs	Good laboratory practices
HPLC	High performance liquid chromatography
Hsp70	70-kDa heat shock proteins
IMAC	Immobilized metal affinity chromatography
MBTH	3-methyl-2-benzothialzolinone hydrazone
MCS	Multiple cloning sites
N/A	Not available
NADH	Reduced nicotinamide adenine dinucleotide
OD_x	Optical density measured at a wavelength of x nm
PCR	Polymerase chain reaction
PDOR	1,3-propanediol oxidoreductase
PEP	Phosphoenolpyruvate
pH	pH value
PTT	Polytrimethylene terephthalate
SDS PAGE	Sodium dodecyl-sulfate (SDS) polyacrylamide gel electrophoresis (PAGE)
TIM	Triosephosphate isomerase

Abstract

The biodiesel sector has witnessed tremendous growth in recent years, leading to a significant increase in glycerol production as a by-product. Addressing the challenge of glycerol valorization is crucial for the sustainability of the biodiesel industry. One promising solution is the conversion of glycerol into more valuable chemicals, such as 1,3-propanediol (1,3-PDO). Microorganisms offer several advantages for this conversion process, including their diverse metabolic pathways and enzymatic capabilities. Key enzymes involved in the 1,3-PDO production pathway include glycerol dehydratase (GDHt), glycerol dehydratase reactivase (GDHtR), and 1,3-propanediol dehydrogenase (1,3-PDDH). The aim of the present research project was to bio-transform glycerol into 1,3-propanediol by cloning and expressing GDHt and 1,3-PDDH in *E. coli.* Additionally, the specific activity of GDHt enzyme and the necessity of GDHtR were investigated. The selected genes dhaB, orfX, and orfZ from *Klebsiella pneumoniae* were utilized for the synthesis of GDHt, GDHtR, and 1,3-PDDH, respectively.

Initial measurements of GDHt's activity revealed detectable levels, which increased upon the addition of GDHtR, indicating the influence of GDHtR on GDHt's activity. However, the interpretation of activity values is complicated by potential interferences from aldehydes or metabolites present in crude cell extracts. To address these complexities, enzyme assays using purified enzymes were performed, but no statistically significant data were obtained. Further investigations are required to optimize the measurement of GDHt activity and address the potential influence of the cofactor B12. Coexpression of GDHt and 1,3-PDDH enzymes, resulted in a reduction of cofactor NADH, indicating the potential conversion of glycerol into 1,3-PDO. Nevertheless, the formation of the product could not be detected, and the decline in NADH could not be solely attributed to the coupled-enzymatic reaction. Additional investigations are required to elucidate possible interferences originating from B12 absorption and cellular components within crude cell extracts that may affect the observed absorbance.

Future prospects involve optimizing experimental conditions, utilizing purified enzymes and alternative substrates, and thoroughly investigating potential interferences in activity measurements. These efforts will contribute to the development of sustainable and efficient strategies of enhancing the efficiency of glycerol bio-transformation processes, facilitating the production of 1,3PDO—a valuable compound with diverse industrial applications.

Popular Science Summary

The production of biodiesel, a type of renewable fuel, has been increasing rapidly, leading to a significant increase in the production of glycerol by-product. Scientists are now looking for ways to use this excess glycerol in a sustainable manner. One exciting solution is to convert glycerol into a valuable chemical called 1,3-propanediol (1,3-PDO). 1,3-PDO is a valuable compound with various applications in industries like manufacturing, textiles, and cosmetics. It can be used to make polyester fibers, which are used in clothing and fabrics, as well as in the production of personal care products like lotions and creams. This conversion process of glycerol into 1,3-PDO can be done by using microorganisms, like bacteria, which have special abilities to transform glycerol into 1,3-PDO.

To make this conversion happen, certain enzymes are involved. Enzymes are special proteins which help carry out specific chemical reactions inside the cells. In the case of glycerol transformation, two key enzymes are responsible for the process: glycerol dehydratase (GDHt) and 1,3-propanediol dehydrogenase (1,3-PDDH). Here's how the transformation of glycerol into 1,3-PDO occurs: First, GDHt takes glycerol and converts it into a different chemical called 3-hydroxypropionaldehyde (3-HPA). Next, 3-HPA goes through another reaction facilitated by 1,3-PDDH, resulting in the formation of 1,3-PDO.

In this research project, these two enzymes were used to transform glycerol into 1,3-PDO. The focus was on studying GDHt and 1,3-PDDH enzymes and how they work together. A common bacterium called *Escherichia coli* (*E. coli*) was used, and the genes responsible for making GDHt and 1,3-PDDH were inserted into these bacteria, to produce the enzymes. When GDHt and 1,3-PDDH were produced together in a single bacterial cell, there was an indication that glycerol was being transformed into 1,3-PDO. However, the actual production of 1,3-PDO couldn’t be detected, and there were other factors affecting the measurements. It was also discovered that GDHt's activity could be increased with the presence of glycerol dehydratase reactivase (GDHR), another important protein. However, measuring GDHt's activity accurately was challenging because there were other components in the bacteria that interfered with the measurement.

To improve these experiments, it is important to optimize the reaction conditions. This means finding the right temperature, pH level, and controlling the presence of oxygen. It is also suggested using purified enzymes, which are enzymes that have been carefully separated from other substances. Additionally, different methods should be explored for measuring the transformation of glycerol into 1,3-PDO. They aim should be to better understand the transformation reaction and find ways to make it more efficient. This research will contribute to developing sustainable ways to utilize glycerol by-product and produce valuable chemicals like 1,3-PDO, which can have various important applications in different industries.

1. Background

Fossil resources are widely used to produce materials and transportation fuels that are essential to our economy and way of life, but there is growing concern about their cost, long-term supply, and effects on global warming and pollution (Hansen et al., 2005). This has resulted in an ongoing search for technologies that create fuels, such as biodiesel, bulk chemicals, and materials from renewable carbon sources (Yazdani & Gonzalez, 2007; Przystałowska et al., 2015b).

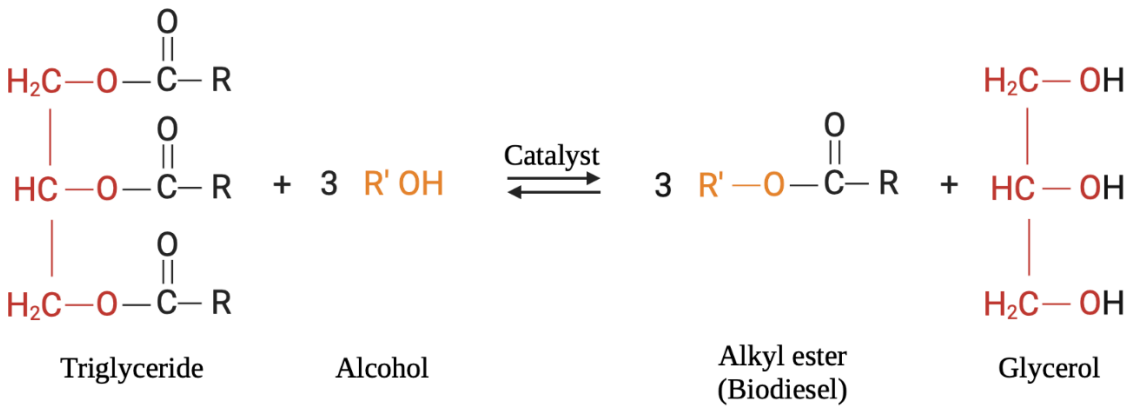

Figure 1.1: Transesterification reaction of biodiesel production. Triglycerides react with alcohol to form alcyl esters and glycerol (Figure adapted from Widayat et al., 2013).

The global production of biodiesel has experienced substantial growth over the years, increasing from 3.9 billion liters in 2005 to 47.4 billion liters in 2019 (Rouhany & Montgomery, 2018; REN21, 2017). This notable expansion can be attributed to the increasing recognition of biodiesel as a renewable and biodegradable fuel that significantly decreases pollutants and toxins released into the atmosphere and the environment. Biodiesel production involves the formation of fatty acid methyl esters via transesterification of triacylglycerols in vegetable or animal fats with short chain alcohols (**Figure 1.1**) (González-Pajuelo et al., 2004; Mu et al., 2006; Przystałowska et al., 2015b). However, along with methyl ester formation, a glycerol fraction is also produced as a by-product, which accounts for 10% of the ester fraction. This means that 100 kgs of crude glycerol is formed for every tonne of biodiesel produced (Yazdani & Gonzalez, 2007; Przystałowska et al., 2015b). In addition to being produced as a side product during biodiesel production, glycerol can also be produced through fat saponification, alcoholic beverage manufacturing, and glucose fermentation (Cheng et al., 2006).

The valorisation of the by-product glycerol fraction poses severe challenges for certain biodiesel businesses in the EU, as glycerol disposal and/or purification is costly (Willke & Vorlop, 2004; Yazdani & Gonzalez, 2007; Jiang et al., 2016). The free fatty acids, methanol, catalyst, soaps, and salt impurities, present in the waste-glycerol fraction associate it with significant costs of evaporation and distillation and render it unusable for the pharmaceutical or cosmetic sectors (Cheng et al., 2006; Przystałowska et al., 2015b). The alternative is for producers to sell the glycerol by-product to a glycerol refinery; however, this is not always feasible due to the complex supply and demand market dynamics. Additionally, freight expenses, which is frequently equal or even surpass the price of the crude glycerol, fall under the purview of the producer. In order to make either of these solutions long-term viable, new

markets for refined glycerol would need to be created as the current glycerol market is unable to handle the surplus amounts produced from the manufacturing of biodiesel (Johnson & Taconi, 2007). The decrease in glycerol price as a result of excessive waste production renders it a competitive raw material in the production of important compounds (Dharmadi et al., 2006; Yazdani et al., 2007; Zhang, 2011; Yang et al., 2012). Using residual glycerol as a carbon and energy source for biotechnological processes would lower the cost of producing biodiesel and increase the proportion of renewable sources employed in the production of useful chemical compounds that are not currently on the market, such as 3-hydroxypropionaldehyde (3-HPA) and 3-hydroxypropionic acid (3-HP), as well as those that are now made from fossil feedstocks (Ragauskas et al., 2006; Chen & Hatti-Kaul, 2017). Furthermore, due to the high degree of reduction in the carbon atoms of glycerol, the conversion of glycerol to pyruvate generates twice as many reducing equivalents compared to the conversion of carbohydrates such as glucose or xylose.. This disparity highlights the potential advantages of utilizing glycerol as a substrate in various metabolic pathways or biotechnological processes, to create "high-value added" products (Dharmadi et al., 2006; Kaur et al., 2012; Kumar et al., 2013).

The growing utilization of 1,3-propanediol (1,3-PDO; $CH_2CH_2(OH)_2$) in various applications has led to an escalating demand for its bio-based production. Therefore, employing microorganisms to produce 1,3-PDO is one of the potential methods for utilising the crude glycerol (Kaur et al., 2012; Ju et al., 2021). The ability to produce 1,3-PDO from non-purified glycerol by-product from the manufacturing of biofuels is a major benefit of the microbial conversion method (Przystałowska et al., 2015b). According to research findings, there is little to no difference between "waste glycerol" and pure glycerol in terms of the growth of 1,3-PDO natural producer bacteria and the generation of 1,3-PDO (Papanikolaou et al., 2004; Ma et al., 2019). Particularly, *K. pneumoniae* demonstrated a significant tolerance to varying concentrations of NaCl, methanol, and oleic acid, which are the primary impurities typically found in crude glycerol (Ma et al., 2019).

1.1. 1,3-propanediol (1,3-PDO)

The compound 1,3-propanediol (1,3-PDO) was initially identified in 1881 by August Freund during the examination of a mixed culture fermentation of glycerol that involved the microorganism *Clostridium pasteurianum.* This discovery marked 1,3-PDO as one of the earliest known products derived from fermentation processes (Saxena et al., 2009). 1,3-PDO is a bifunctional organic compound characterized by its colorless and viscous liquid state. It is nonflammable, exhibits low toxicity, and demonstrates easy solubility in water, alcohol, and ether (Ju et al., 2021; Marçal et al., 2009).

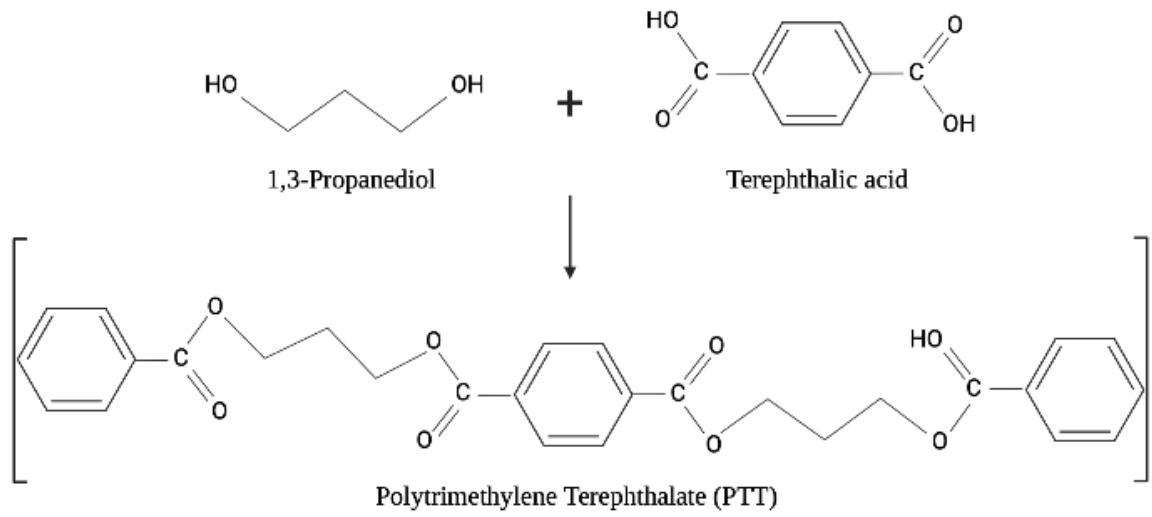

Figure 1.2: Condensation reaction of 1,3-propanediol and terephthalic acid for the synthesis of polytrimethylene terephthalate (PTT) polyester. The molecular structure of the participating compounds is illustrated (Figure adapted from Saxena et al., 2009).

1,3-PDO can be employed in the synthesis of heterocyclic compounds as a versatile intermediate and has applications in the manufacturing of polymers because of the two hydroxyl groups found at the 1 and 3 positions (**Figure 1.2**, top part) (Biebl et al., 1999). 1,3-Propanediol-based polymers have improved washfastness and are more strain-resistant (Saxena et al., 2009). Polyesters, polyethers, and polyurethanes are among the most notable examples of 1,3-PDO-based polymers, that are created by polycondensation reactions of petrochemical compounds (Marçal et al., 2009; Ju et al., 2021). For instance, polytrimethylene terephthalate (PTT) (**Figure 1.2**), a polyester synthesized through the condensation reaction of 1,3-propanediol and terephthalic acid, has dramatically increased the demand for 1,3-propanediol (Kurian, 2005). PPT is a polymer with superior stretching and stretch recovery properties and significant application potential in the manufacture of textiles, carpets, and upholstery (Witt et al., 1994; Kurian, 2005).

The 1,3-PD-based polyesters' biodegradable properties, improved light stability, and solubility in commonly used solvents expand their already wide range of uses (Witt et al., 1994; Umare et al., 2007). These applications encompass laminates, solvents, moldings, adhesives, resins, detergents, cosmetics, deodorants, and other end uses (Yu et al., 2010). Moreover, 1,3-PD finds utility as a solvent in water-based inks, including ink-jet and screen inks. 1,3-PD is a crucial intermediate in the synthesis of organic compounds and is employed in a wide range of products, including fragrances, insect repellents, vitamin H and immunosuppressive medications. Consequently, it is of highly importance to produce 1,3-PD that is biobased (Kaur et al., 2012).

1.2. Chemical Synthesis of 1,3-PDO

The chemical process for producing 1,3-PDO involves either the acrolein route or the ethylene route. Degussa (currently owned by DuPont), and Shell, commercialized these methods of chemical synthesis, respectively (Liu et al., 2010). In particular, the first method (**Figure 1.3**) involves the hydration of acrolein, which is derived from the catalytic oxidation of propylene. This process occurs at moderate temperature and pressure and leads to the formation of 3-hydroxypropionaldehyde (3-HPA) (Zeng & Biebl, 2002). Subsequently, 3-HPA undergoes hydrogenation to generate 1,3-propanediol (1,3-PDO), employing a rubidium catalyst under high-pressure conditions (90 bar). The maximum yield of 1,3-PDO achieved in this method does not exceed 65% (Arntz & Wiegand, 1991; Zeng & Biebl, 2002; Kurian, 2005).

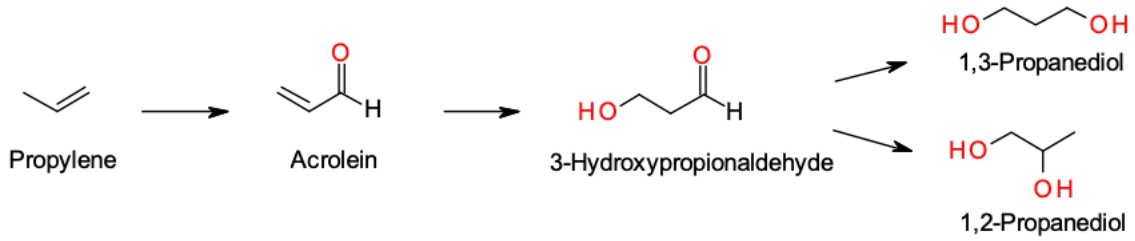

Figure 1.3: Degussa 1,3-propanediol (1,3-PDO) chemical synthesis process from propylene through the intermediate compound 3-hydroxypropionaldehyde (Rezaei, 2013).

As for the alternative approach (**Figure 1.4**), it involves the hydroformylation process of ethylene, utilizing carbon monoxide and hydrogen at a pressure of 150 bars. This process converts ethylene oxide, obtained through the oxidation of ethylene, into 3-hydroxypropanal. Subsequently, 3-hydroxypropanal is extracted into the aqueous phase and further hydrogenated to produce 1,3-propanediol (1,3-PDO). The hydrogenation reaction is facilitated by a nickel catalyst under high-pressure conditions and can achieve a final yield of 80% for 1,3-PDO (Lam et al., 1997; Zeng & Biebl, 2002; Sun et al., 2018).

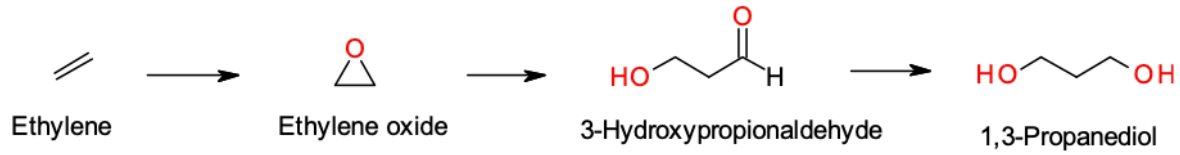

Figure 1.4: Shell 1,3-propanediol (1,3-PDO) chemical synthesis process) from ethylene utilizing 3-hydroxypropionaldehyde as an intermediate compound (Rezaei, 2013).

The problems associated with these traditional procedures include the use of hazardous solvents, the particularly poor yields (5–15% w/w) for 1,3-PDO production and the by-product formation, such as 1,2-propanediol (Chaminand et al., 2004; Jun et al., 2009). Further disadvantages are the high pressures and temperatures that are required for the hydroformylation and hydrogenation reactions to occur, the employment of expensive catalysts (such as Iridium, Chromium and Silver), and the release of

hazardous intermediates (such as 3-hydroxypropyonaldehyde) that are damaging to the environment. Lastly, the cost of 1,3-PDO production using the conventional chemical process is high, and not price competitive (Liu et al., 2010; Ju et al., 2021).

The biological conversion of glycerol to 1,3-PDO using microorganisms is an environmentally friendly and cost-effective process compared to chemical conversion because it requires less energy, has milder reaction conditions, and produces a higher yield of 1,3-PDO than chemical conversion (Jun et al., 2009).

1.3. Microbial Synthesis of 1,3-PDO

The anaerobic and microaerophilic bacterial strains *Klebsiella pneumoniae*, *Klebsiella oxytoca*, *Klebsiella planticola* (Slininger et al., 1983), *Clostridium butyricum, Clostridium pasteurianum (*Luers et al., 2006)*, Citrobacter freundii* (Mickelson & Werkman, 1940; Daniel et al., 1995a), and *Enterobacter agglomerans* (Barbirato et al., 1995), as well as microorganisms of the genus *Lactobacillus* (*Lactobacillus brevis*, *L. reuteri*, *L. sakei*, *L. plantarum*, and *L. buchneri*) (Singh et al., 2021) have been identified for 1,3-PDO biological production from glycerol fermentation (Biebl et al., 1999; Marçal et al., 2009; Saxena et al., 2009; Gundogan, 2014). With the use of renewable glycerol rather than non-renewable petroleum, this bioconversion method offers a safe, cost-effective way to produce commercially important 1,3-PDO (Ju et al., 2021). Furthermore, the microorganisms are cultivated under standard temperature and pressure conditions, resulting in minimal or no generation of toxic by-products (Kaur et al., 2012). Although, with the exception of lactic acid bacteria, the named microbiological strains are completely anaerobic, pathogenic, or genetically modified (Saxena et al., 2009; Ju et al., 2021). Therefore, special equipment and safety precautions are required for their handling (Saxena et al., 2009; Ju et al., 2021).

Extensive research has been conducted on the microorganisms *Klebsiella pneumoniae* and *Clostridium butyricum*, primarily due to their notable characteristics such as substrate tolerance, high yield, and productivity. (Liu et al., 2007). *Klebsiella pneumoniae* is of great importance because of its versatile carbon regulation, ability to reduce comparable fluxes under various settings, and higher production when compared to other strains. It is commonly present in diverse environments such as carbohydrate-rich wastewater, surface water, soil, plant products, fresh vegetables, sugar cane, and grains. *K. pneumoniae* is classified as a facultative anaerobic, gram-negative, non-spore-forming, non-motile member of the Enterobacteriaceae family (Gundogan, 2014; Ashurst & Dawson, 2023). *It* is characterized by the presence of straight rod-shaped cells, with diameters ranging from 0.3 to 1.0 mm and lengths ranging from 0.6 to 6.0 mm. These cells typically occur as individual cells, pairs, or short chains and can develop a gelatinous encapsulation under specific conditions (Gundogan, 2014; Ashurst & Dawson, 2023). While *K. pneumoniae* can thrive on glycerol in aerobic, microaerobic, and anaerobic conditions, *C. butyricum* is typically an anaerobic microorganism. However, *K. pneumoniae* is a pathogen that has been linked to pneumonia in patients with diabetes or alcohol use disorders, which suppresses its industrialization (Sun et al., 2018; Ashurst & Dawson, 2023).

1.4. 1,3-PDO Metabolic Pathway

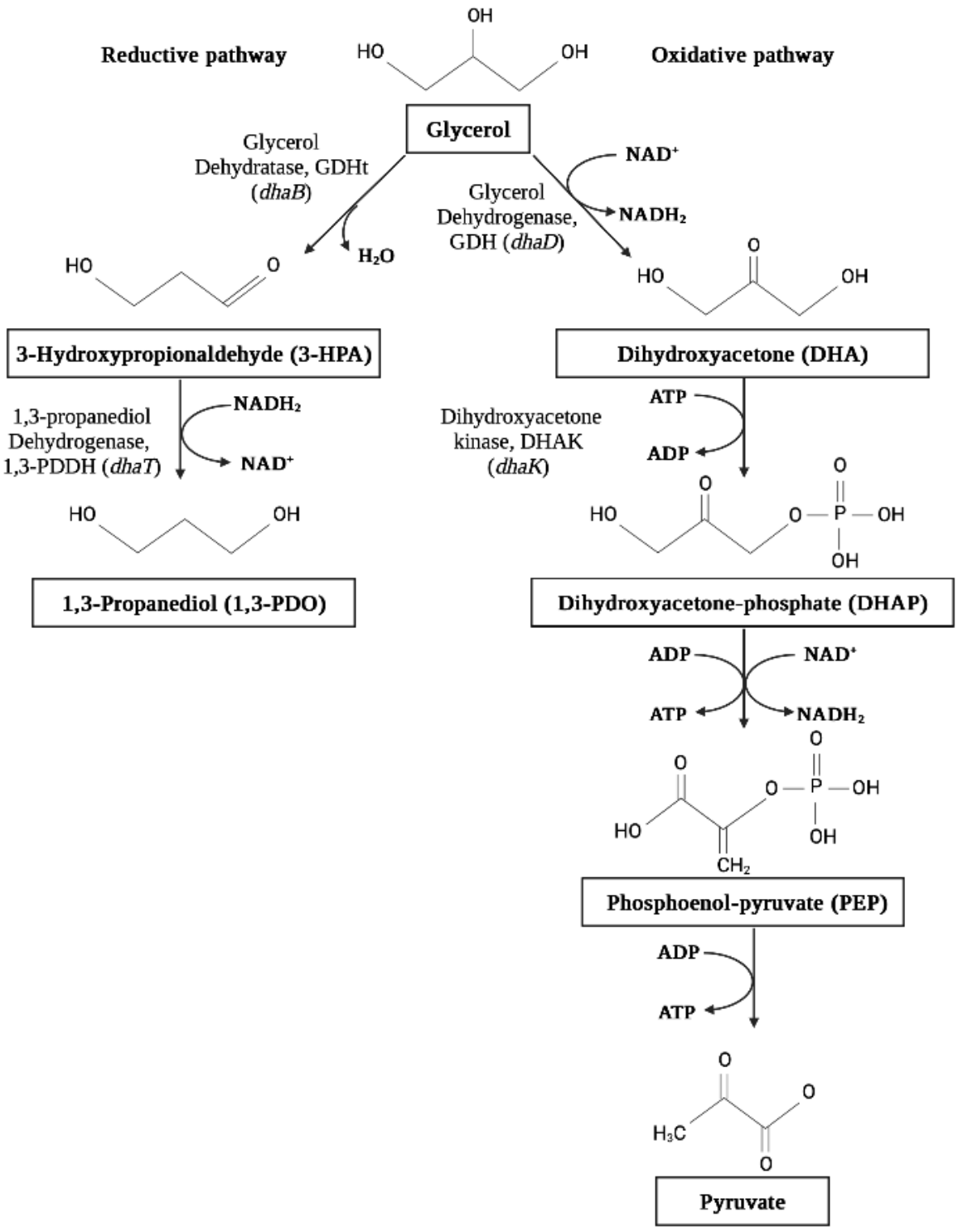

Figure 1.5: Glycerol catabolism pathways from Klebsiella pneumoniae. On the right side of the figure, the oxidative pathway is depicted, wherein glycerol undergoes a series of enzymatic reactions leading to the formation of pyruvate. On the left side, the reductive pathway is shown, which includes the enzymes glycerol dehydratase and 1,3-propanediol dehydrogenase, ultimately resulting in the production of 1,3-propanediol.. The names of the genes that code for the enzymes of both pathways are presented within brackets (Figure adapted from Przystałowska et al., 2015b).

Like the other 1,3-PDO natural producers, *Klebsiella pneumoniae* uses two distinct parallel routes to metabolize glycerol (**Figure 1.5**). The first is an oxidative pathway in which glycerol is transformed into dihydroxyacetone (DHA) by a NAD-dependent glycerol dehydrogenase (GDH) and is phosphorylated by the enzyme dihydroxyacetone kinase (DHAK) before being further transformed into pyruvate, glyceraldehyde-3-phosphate, and phosphoenolpyruvate to enter the Krebs cycle (Ahrens et al., 1998; Sun et al., 2003). Using a second reductive pathway, the reduced cofactors produced during the conversion of glycerol to DHA can be recycled. Two enzymes are involved in this pathway: a coenzyme B12-dependent glycerol dehydratase (GDHt), which first converts glycerol to 3-hydroxypropionaldehyde (3-HPA), and a reduced nicotinamide adenine dinucleotide-dependent 1,3-propanediol dehydrogenase (1,3-PDDH), which turns this latter substance into 1,3-PDO (Ahrens et al., 1998; Cheng et al., 2006; Marçal et al., 2009; Gundogan, 2014).

Along with 1,3-PDO, 3-hydroxypropionic acid (3-HP) is produced through the oxidation of 3-HPA by *K. pneumoniae* and a few other bacteria, including *L. reuteri* and *L. collinoides*. A coenzyme A (CoA) -dependent route is particularly used by natural strains of *K. pneumoniae* to generate 3-HP from glycerol (Kumar et al., 2013). In this pathway, CoA-dependent propionaldehyde dehydrogenase (also known as propanediol utilization protein, PduP) catalyzes a sequence of reactions that result in the conversion of 3-HPA to 3-HP (Luo et al., 2012). However, it was discovered that a recombinant *K. pneumoniae* strain, which overexpressed the aldehyde dehydrogenase (ALDH) PuuC, had the capability to efficiently produce 3-hydroxypropionaldehyde (3-HP) from glycerol through a CoA-independent pathway (Ashok et al., 2011). The NAD^+-dependent ALDH oxidizes 3-HPA directly to 3-HP in this CoA-independent route. The oxidative pathway of glycerol metabolism and/or an electron transport chain are used to regenerate the NAD^+ cofactor. This 3-HP production route can make use of the various ALDHs found in many bacteria and does not produce ATP or require coenzyme A. However, it is still unclear how this mechanism for 3-HP synthesis in wild bacteria works (Kumar et al., 2013).

1.5. The dha Regulon

According to Forage and Lin (1982), the four enzymes glycerol dehydrogenase (GDH), dihydroxyacetone kinase (DHAK), glycerol dehydratase (GDHt), and 1,3-propanediol dehydrogenase (1,3-PDDH), are co-expressed and their expression is stimulated by dihydroxyacetone or glycerol (Forage & Lin, 1982; Morita et al., 2008). Tong et al. (1991), reported that the genes for these four enzymes are arranged on the chromosome in a cluster in *K. pneumoniae*, named dha regulon (**Figure 1.6**) (Tong et al., 1991).

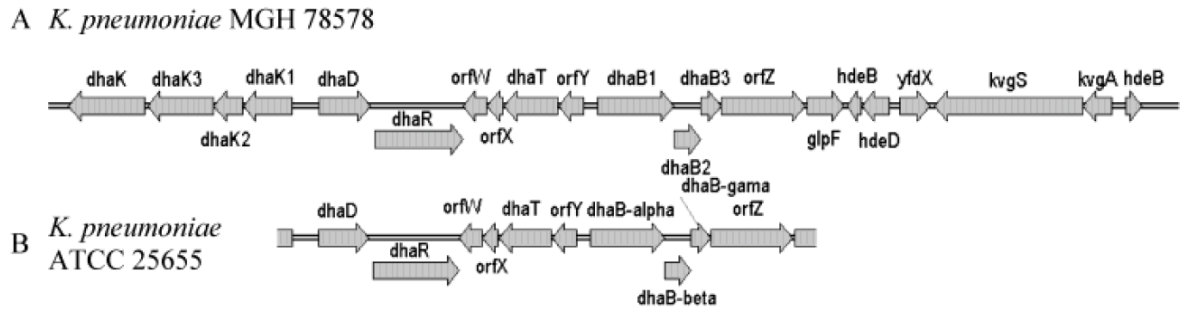

Figure 1.6: dha regulon and related genes in two different Klebsiella spp. (A) Klebsiella pneumoniae MGH 78578. (B) Klebsiella pneumoniae ATCC25655 (Sun et al., 2003).

The dha regulon has been partly sequenced in *K. pneumoniae*, *Citrobacter freundii*, *Clostridium pasteurianum*, and more recently, *Clostridium butyricum* (Sun et al., 2003). Common parts of the dha regulon in these microorganisms include *dhaB1*, *dhaB2*, *dhaB3*, *dhaT*, *orfX*, *orfZ*, *orfW*, and *orfY*. All of them are a part of the reductive pathway for glycerol usage, with the exception of *orfW* and *orfY*, whose roles are unknown (Sun et al., 2003). The two enzymes of the reductive pathway of glycerol metabolism, GDHt and 1,3-PDDH, are encoded, respectively, by the *dhaB* (B1, B2, and B3) and *dhaT* genes. The small and large subunits of an activator of GDHt are encoded by the genes *orfX/ dhaG* and *orfZ/ dhaF*, respectively (Seifert et al., 2001; Kumar & Park, 2018). Additionally, the *dhaT* and *dhaB* genes of the dha regulon have a positive regulatory protein encoded by the *dhaR* gene. *K. pneumoniae's* DhaR may be able to detect intracellular concentrations of significant physiological factors like redox potential or energy charge and function as an effector to start the transcription of dha regulon genes. (Sun et al., 2003).

In addition to the dha regulon's previously identified genes in *K. pneumoniae* ATCC 25655, the reconstructed dha regulon of *K. pneumoniae* MGH 78578 encodes a number of novel dha regulon-related genes. Newly discovered genes include the ORFs *dhaK*, *dhaK1*, *dhaK2*, and *dhaK3* (Sun et al., 2003). In *K. pneumonia*, *dhaK* encodes the ATP-dependent dihydroxyacetone kinase (DHAK I) (Ruch & Lin, 1975). *DhaK1*, *dhaK2*, and *dhaK3* share a high degree of identity with the *E. coli* genes encoding the three soluble protein subunits of a dihydroxyacetone kinase (DHAK II) that utilizes phosphoenolpyruvate (PEP) rather than ATP as the phosphoryl donor (Gutknecht et al., 2001). Moreover, the *dhaD* gene encodes GDH, the other enzyme of the oxidative pathway. The *glpF* gene, which codes for a glycerol transport facilitator, as well as numerous other global regulation-related genes (*hdeBD*) and genes encoding a two-component signal transduction system (*kvgA* and *kvgS*), are located in the right-hand half of the DNA fragment. The common dha regulon gene is discovered close to *glpF* gene that encodes glycerol transport facilitator. It is unknown if glpF is a member of the dha regulon and is coordinatedly regulated with the dha genes (Sun et al., 2003).

1.5.1. Glycerol dehydratase (GDHt)

Through a radical process in the presence of monovalent cations and 5′-deoxyadenosylcobalamin (coB12), glycerol dehydratase (GDHt, EC 4.2.1.30) converts glycerol to 3-HPA (Liao et al., 2003a; Jiang et al., 2016). Other small vicinal diols can also be converted to the corresponding aldehydes at slower rates (Liao et al., 2003a). GDHt is a member of the family of coB12-dependent “eliminases” that catalyze the removal of water or ammonia from their substrates (Golding & Buckel, 1998). This family also includes the enzymes diol dehydratase (DDH), ribonucleotide reductase, and ethanolamine ammonia lyase (Liao et al., 2003a).

GDHt derived from 1,3-PDO-producing bacteria is classified into three types. The first type, which is dispersed throughout the cell membrane, does not rely on coenzyme B12 and is oxygen-sensitive. A representative of this class is the ethylene glycol dehydrogenase of *C. glycolycum*. The second category of GDHt enzymes, found in *Klebsiella pneumoniae*, *Citrobacter species*, and *Clostridium pasteurianum*, relies on the presence of coenzyme B12 for its activity. These enzymes display a capacity to withstand oxygen exposure, while undergoing self-inactivation in the presence of the glycerol substrate. Lastly, the third class, which is represented by the *C. butyricum’s* GDHt, does not rely on coenzyme B12, is oxygen-sensitive, is suicidally inactivated by the substrate glycerol, and is reactivated with the aid of *S*-adenosyl methionine (SAM) (Jiang et al., 2016).

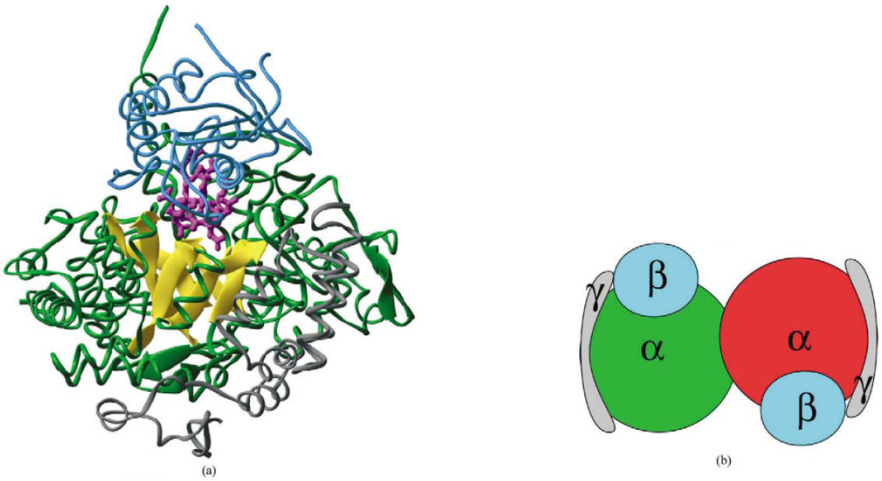

Figure 1.7: (a) A ribbon diagram of the GDHt's αβγ trimeric structure from Klebsiella pneumoniae. The central β barrel that encloses the active site is highlighted in yellow, while the α subunit is colored green. Cyan and Gray are used for the β and γ subunits, respectively. Magenta represents the B12 cofactor. (b) A graphic illustration of the GDHt's $(\alpha\beta\gamma)_2$ assembly (Adapted from Liao et al., 2003a).

The GDHt enzyme from *K. pneumoniae* comprises of three different subunits α (large, 60.7 kDa),β (medium, 21.3 kDa) and γ (small, 16.1 kDa), with subunit composition $\alpha_2\beta_2\gamma_2$ (**Figure 1.7b**) (Yamanishi et al., 2002; Kumar & Park, 2018). It is built up as a dimer, consisting of two αβγ heterotrimers (**Figure 1.7a**) (Liao et al., 2003a). The genes *dhaB1*, *dhaB2*, and *dhaB3*, respectively, code for each of the three distinct subunit types (Sun et al., 2003). The TIM (triosephosphate isomerase) barrel structure and the central β barrel found in the α subunit include the substrate binding site as well as the binding site for the vital K^+ ion, respectively (Liao et al., 2003b). Similar to other diol dehydratases, the glycerol dehydratase of *K. pneumoniae* contains the coenzyme B12 in the reaction center, entirely buried between the central β barrel's open end and the β subunit (Daniel et al., 1998; Liao et al., 2003b). The binding of cobalamin shields the active site from solvent molecules (Toraya, 2000). The elongated γ subunit is positioned adjacent to the α subunit, running along its side, and exhibits limited interaction with the β subunit within the same trimeric structure (Liao et al., 2003a).

1.5.1.1. Glycerol dehydratase (GDHt) inactivation

The quick inactivation of GDHt during enzymatic turnover with its' natural substrate glycerol is a crucial characteristic of the enzyme (Toraya et al., 1976; Liao et al., 2003a; Sun et al., 2003). The loss of the intermediate radical from the active site is what triggers this action, which keeps the total amount of glycerol turnovers catalyzed by GDH to approximately 100,000. The firmly bound inactive cofactor cob(II)alamin remains in the enzymes' active site but is unable to start more radical reactions (Honda et al., 1980; Liao et al., 2003a).

Moreover, it has been widely reported that oxygen significantly inactivates GDHt (Honda et al., 1980; Toraya, 2000; Doitomi et al., 2012). The Co-C link between cobalt and the adenosyl moiety of the GDHt core enzyme breaks down when the GDHt holoenzyme is exposed to oxygen, causing irreparable damage to the coenzyme B12 (Schwartz & Frey, 2007; Jiang et al., 2016). When glycerol is employed as the substrate, this damage is exacerbated (Sankaranarayanan et al., 2017).

1.5.2. Glycerol dehydratase reactivase (GDHtR)

The ability of the glycerol dehydratase reactivase (GDHtR), the expression product of the *orfX/ dhaG* and *orfZ/ dhaF* genes, to reactivate glycerol-deactivated or oxygen-deactivated GDHt as well as effectively prevent the deactivation of the GDHt from glycerol in the presence of coenzyme B12, ATP, and Mg^{2+} is supported by increasing amounts of experimental data (Mori et al., 1997; Sun et al., 2003; Liao et al., 2003a). The reactivase uses the energy from ATP hydrolysis to catalyze the exchange of cob(II)alamin for intact coenzyme B12 from the medium (Honda et al., 1980; Liao et al., 2003a). In this process, the function of ATP hydrolysis is to cause conformational changes in the reactivase that regulates its affinity for the apoenzyme (Liao et al., 2003b).

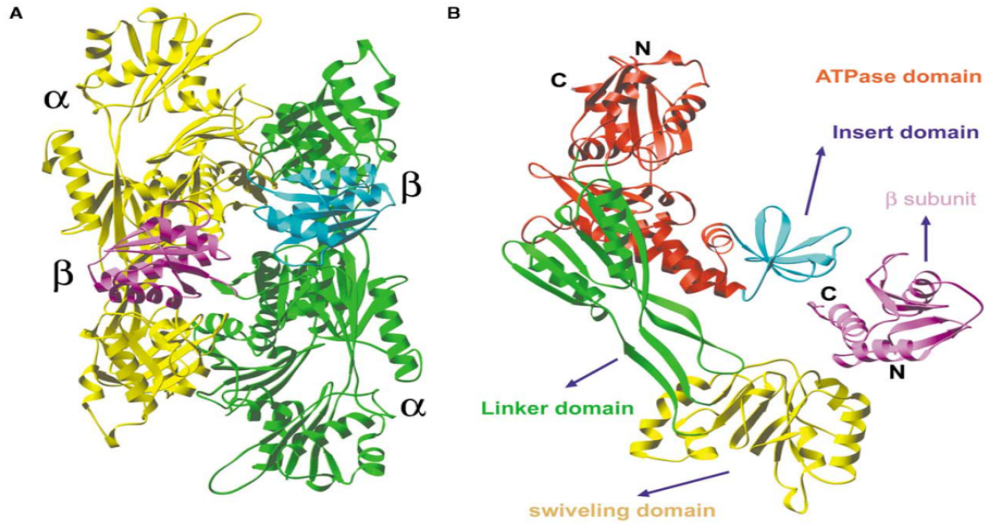

Figure 1.8: (a) Ribbon diagram illustrating the heterotetrameric structure α2β2 of glycerol dehydratase reactivase (GDHtR) from Klebsiella pneumoniae. The α and β subunits are depicted in different colors: α subunit (yellow and green), β subunit (cyan and purple). (b) Ribbon diagram illustrating the αβ heterodimer of GDHtR. The α subunit consists of distinct folding domains represented by different colors: ATPase domain (red), linker domain (green), swiveling domain (yellow), and insert domain (cyan). The β subunit is colored purple. (Adapted from Liao et al., 2003b).

According to the crystal structure, first obtained by Liao et al., (2003b) GDHtR comprises of two αβ heterodimers, making it a heterotetramer (**Figure 1.8a**). The α subunit is approximately 110 Å long (63 kDa) and has one independent folding unit at one end of the molecule and two folding units at the other. The central region of the molecule is primarily made up of two medium-sized helices, one short β strand, and four long, twisted β strands. The globular, 30-Å diameter (14 kDa) β subunit is small and spherical in shape. Through interactions with the folding domains on both ends of the β subunit, it interacts with the α subunit (Liao et al., 2003b; Kumar & Park, 2018). The GDHtR $\alpha_2\beta_2$ complex's crystal structure reveals that it shares structural similarities with two separate classes of molecular chaperones, 70-kDa heat shock proteins (Hsp70) and GroEL. The reactivase has been proposed as a brand-new class of molecular chaperone designed specifically for reactivating inactive enzymes (Mori & Toraya, 1999; Liao et al., 2003b).

1.5.3. 1,3-PDO dehydrogenase (1,3-PDDH)

1,3-PDO dehydrogenase (1,3-PDDH) is a crucial enzyme in the microbial synthesis of 1,3-PDO, which is formed by hydrogenation of 3-HPA. The 1,3-PDDH enzyme is encoded by the *dhaT* gene in *K. pneumoniae and* belongs to the iron-containing family III of metal-dependent polyol dehydrogenases (Ruzheinikov et al., 2001; Jiang et al., 2016). While some members of this protein family, such as *Escherichia coli* propanediol dehydrogenase, have been shown to require Fe^2 for their enzymatic activity (Montella et al., 2005), others, like *Bacillus stearothermophilus* glycerol dehydrogenase, showed a dependence on Zn^2 (Ruzheinikov et al., 2001). Additionally, some members of this family require cofactors like NAD^+ or $NADP^+$ (Bouvet et al., 1995; Marçal et al., 2009).

The 1,3-PDO serves as a natural substrate for 1,3-PDDH, and NAD^+ is required as a cofactor in the catalytic step. It was shown that the enzyme was able to catalyze other substrates, including 1,4-butanediol, 1-butyl alcohol, 1-propanol, glycerol, and 1,2-propylene glycol (Jiang et al., 2016). The ideal substrate for the catalytic reduction reaction of the 1,3-PDDH from *C. butyricum* E5 and *C. freundii* DSM 30040 was 3-HPA, whereas the ideal substrate for the catalytic oxidation reaction was 1,3-PDO (Daniel et al., 1995b; Jiang et al., 2016; Malaoui & Marczak, 2000). Divalent metal ions have the ability to activate the 1,3-PDDH enzyme, however an enzymatic direct activator has not been identified (Jiang et al., 2016). According to Johnson & Lin, (1978), Mn^{2+} and Fe^{2+} can reactivate the 1,3-PDDH from *K. pneumoniae* (Johnson & Lin, 1987). Similarly, on the 1,3-PDDH from *C. freundii* DSM 30040, Mn^{2+} and Fe^{2+} had an activating effect (Daniel et al., 1995b). The 1,3-PDDH from *C. butyricum* E5 demonstrated the highest enzyme activity only in the presence of Mn^{2+} while it decreased by 60–90% with other cations (Malaoui & Marczak, 2000).

The characterization of the 1,3-PDDH enzyme from *Klebsiella pneumoniae* through size exclusion chromatography has revealed its oligomeric nature, existing as either a hexamer or octamer. Each monomer's molecular weight was 43 kDa. Furthermore, the enzyme has been observed to be sensitive to divalent cation chelators, such as ethylenediaminetetraacetic acid (EDTA), which inhibit its activity. Additionally, the presence of reactive oxygen species has been found to deactivate the enzyme (Johnson & Lin, 1987; Marçal et al., 2009; Kumar & Park, 2018). More recently, Marçal et al. (2009) used X-ray crystallography to identify the 3D structure of 1,3-PDDH from *K. pneumoniae*. Their investigation has shown a decameric configuration, which may be important for the catalytic activity of this protein in solution and differs from the structures of other members of this family of enzymes (Marçal et al., 2009). The main benefits of big protein assemblies come from biophysical phenomena including structural function, cooperativity, stability against denaturation, and surface area reduction (Goodsell & Olson, 2000). The solvent surface accessible area on the decamer was substantially lower when compared to the total of the equivalent regions on the isolated monomers, according to a thorough examination of the 1,3-PDDH structure (Marçal et al., 2009). As a result of the decrease in the hydration sphere, the enzyme has greater stability in its decameric form. The increase in the system's catalytic capabilities has also been associated with the decrease in solvent-accessible area in multimeric enzymes. Reduced accessible area enhances substrate diffusion to enzyme active sites, ultimately resulting in improved interactions (Nooren & Thornton, 2003; Han et al., 2007; Marçal et al., 2009).

2. Aim of the Study

The aim of the present research project was to clone and express the genes encoding glycerol dehydratase (GDHt) and 1,3-propanediol dehydrogenase (1,3-PDDH) in *E. coli* to develop an engineered microbial system to bio-transform glycerol into 1,3-propanediol. Additionally, the necessity of the glycerol dehydratase reactivase (GDHtR) was investigated. Several distinct genes are known to be involved in the synthesis of 1,3-propanediol. The *dhaB* gene for the GDHt, the *orfX and orfZ* genes for its' reactivase and the *dhaT* gene for the 1,3-PDDH were selected, all originating from *K. pneumonia.* In addition, the objective was to assess the specific activity of the GDHt enzyme expressed in an inhouse *E. coli* strain as well as to examine the enzyme's capacity to transform glycerol into 1,3-PDO in the presence of 1,3-PDDH, with or without the GDHtR enzyme.

3. Materials and Methods

The primer sequences utilized in this study can be found in **Table A1**, while the enzymes and kits employed are listed in **Table A2**, both of which are included in the appendix. Additionally, the appendix **Tables A3**, **A4**, and **A5**, provide further information on the commercially available chemicals, software, and devices utilized in the study. In particular, **Table A3** contains the buffer recipes employed throughout the study, ensuring accurate replication of the experimental conditions in future studies. **Table A4** includes information on other chemicals used, excluding those used for buffers. Lastly, **Table A5** lists all the equipment and software used throughout the study, providing a comprehensive overview of the experimental setup.

In addition to the procedures and protocols described in the following subchapters, strict adherence to good laboratory practices (GLPs) was maintained throughout the study (OECD). GLPs encompass a set of guidelines and principles aimed at ensuring the reliability, integrity, and reproducibility of scientific research. These practices include meticulous documentation of procedures, accurate record-keeping, proper handling and disposal of hazardous materials, regular calibration and maintenance of laboratory equipment, and the implementation of appropriate quality control measures. To ensure sterility, all procedures were conducted under sterile conditions within a class II laminar flow biological safety cabinet (Heto-Holten). Moreover, prior to usage, all surfaces were thoroughly cleaned with 70% ethanol to maintain a sterile environment and minimize contamination risks.

3.1. Bacterial Strains, Plasmids, and Cultivation conditions

Tables 3.1 and **3.2** provide a comprehensive list of the bacterial strains and plasmids utilized in this research. By default, *E. coli* strains were cultured on Luria-Bertani (LB) agar plates overnight at a temperature of 37°C or in LB broth liquid cultures with continuous shaking at 220 rpm, overnight at 37°C. The antibiotics kanamycin (50 µg x mL^{-1}), and streptomycin (50 µg x mL^{-1}) were added in the specified concentrations for the selection of recombinant strains transformed with the pET-28a(+) and pCDFDuet™-1 vectors, respectively. Particularly, kanamycin was used for the recombinant strains containing the pET Centrifugation at 4500 x g, 4°C for 10 min was used to harvest the cells, followed by a washing step using a 50 mM resuspension buffer (K_2HPO_4 32.72 mM, KH_2PO_4 2.283 mM, KCl 50 mM) at pH 8.0. Plasmid-containing or plasmid-free bacterial strains were kept at -80°C after mixing a sample of growing or saturated culture with 0.1 vol. 40% (v/v) glycerol.

Table 3.1: Bacterial strains that were used in this work. The strains' phenotype, genotype, description, and source are indicated.

Strain	Phenotype; Genotype	Description	Source
E. coli BL21 (DE3) Competent cells	T7 Expression host; *E. coli* B F– dcm ompT hsdS(r – m –) gal λ(DE3)	A prophage T7 RNA polymerase gene-containing strain that is regulated by the lacUV5 promoter. High-level expression and simple induction of non-toxic proteins can be achieved by this all-purpose derivative.	Agilent Technology, USA
E. coli DH5α	Cloning host; F-Φ80lacZΔM15 Δ(lacZYA-argF) U169 recA1 endA1 hsdR17(rk-, mk+) phoA supE44 thi-1 gyrA96 relA1 λ-	A strain with slow growth. After one day at 37°C it produces small colonies. Ideal for transforming DNA from ligation reactions and creating competent cells	Sigma-Aldrich, USA

Table 3.2: Plasmids that were used in this work. Some relevant features including antibiotic resistance, promoter and indicated usage as well as the source for each plasmid are indicated.

Plasmid	Relevant features[1]	Source & Reference
pCDFDuet™-1	Bacterial vector with a CloDF13 (CDF) origin for the co-expression of two genes in two different multiple cloning sites (MCS-1 and MCS-2). Each multiple cloning site is preceded by a T7 promoter. Spt^r & Str^r (© 2023 SnapGene, 2023a).	Novagen, USA (**Figure A1**)
pCDFDuet™-1_dhaT	pCDFDuet™-1 transformed with codon optimized *DhaT* under the control of a T7 promoter, for the expression of 1,3-PDDH. Spt^r & Str^r	Previous study of the group (DSP)
pET-28a(+)	Bacterial vector for the expression of thrombin-sited, 6xHis-tagged proteins, under the control of a T7 promoter. *lac* operator, Kan^r (© 2023 SnapGene, 2023b).	Twist Bioscience, USA (**Figure A2**)
pET-28a(+)_dhaB	pET-28a(+) transformed with codon optimized *dhaB* (three subunits) under the control of a T7 promoter, for the expression of GDHt. *lac* operator, Kan^r	Twist Bioscience, USA
pET-28a(+)_orfX/orfZ	pET-28a(+) transformed with codon optimized *dhaR* under the control of a T7 promoter, for the expression of GDHtR (two subunits). *lac* operator, Kan^r	Twist Bioscience, USA

3.2. Introduction and Expression of GDHt (*dhaB*), GDHtR (*orfX/orfZ*), and 1,3-PDDH (*dhaT*) in *E. coli*

Codon-optimized *dhaB*, *orfX/orfZ*, and *dhaT* genes that were integrated in pET-28a(+) vector, were ordered from the company Twist Bioscience (USA). In previous studies conducted by the research group, the *dhaT* gene was ligated into the MCS-2 position of the pCDFDuet™-1 vector using the Gibson Assembly technique. The cells that underwent transformation were preserved in a solution containing 25% glycerol at a temperature of -80°C.

The experimental procedure employed in the present degree project involved several steps. Initially, chemically competent *E. coli* BL21(DE3) cell cultures were prepared. These cultures were then genetically engineered by introducing three different plasmids: pET-28a(+)_*dhaB*, pET-28a(+)_*orfX/orfZ*, and pCDFDuet™-1_*dhaT*. The *dhaB* and *dhaT* containing plasmids were also co-transformed in the same *E. coli* cells. The transformed cells were then cultivated until they reached an optical density of 0.6 at a wavelength of 600 nm. Subsequently, the cells were induced by adding 0.5 mM IPTG. The bacteria were harvested, and the soluble fraction, which is expected to contain the main protein fragment, was obtained through lysis via sonication and centrifugation. The presence of the respective proteins was confirmed using SDS-PAGE, and the activity of the GDHt protein was assessed using the 3-methyl-2-benzothialzolinone (MBTH) method. Furthermore, the ability of GDHt and 1,3-PDDH to convert glycerol substrate into 1,3-PDO was tested, and the samples were analyzed using HPLC. The specific details of the experimental procedure can be found in the following subchapters.

[1] Spt^r, Spectinomycin resistant; Str^r, Streptomycin resistant; Kan^r, Kanamycin resistant

3.2.1. Chemically competent *E. coli* BL21 (DE3) and *E. coli* DH5a cells

The rubidium chloride approach described by Mülhardt & Beese (2007) was used to prepare chemically competent *E. coli* BL21 (DE3) and *E. coli* DH5a cells for transformation experiments (Mülhardt & Beese, 2007). The entire procedure was conducted following sterile conditions to ensure the integrity and purity of the cells.

After plating the cells on LB agar plates and overnight incubation at 37°C, a single colony was used to inoculate a 4 mL starter culture of liquid LB-media without antibiotics. The starter culture was incubated overnight, shaking at 225 rpm at 37°C. On the next day, the started culture was used to inoculate a growth culture at 1:100 ratio (250 µL of starter culture into 25 mL of LB-media) and incubated shaking at 225 rpm from 2 to 3 hours, until the culture demonstrated an OD_{550} nm of 0.45 to 0.55, to obtain cells approximately in the mid-exponential growth phase. Following, the culture was split into 50 mL falcon tubes, and placed for 10 min on ice before harvesting by centrifugation (Sigma-Aldrich) for 10 min at 4,000 rpm and 4°C. After removal of the supernatant, the pellet was resuspended in 10 mL of ice-cold TFB I (10 mM $CaCl_2 \cdot 2H_2O$, 15% [v/v] glycerol, 50 mM $MnCl_2 \cdot 4H_2O$, 30 mM potassium acetate, 100 mM $RbCl_2$) and put on ice for 10 minutes. A second centrifugation under the same conditions followed, the supernatant was discarded and the cell pellet was resuspended in 800 µL of ice-cold TFB II (75 mM $CaCl_2$, 15% [v/v] glycerol, 10 mM MOPS, 10 mM $RbCl_2$). Aliquots of 50 µL were made using pre-chilled Eppendorf tubes of 1 mL and they were stored in the freezer at −80°C.

3.2.2. Transformation with pET-28a(+)_*orfX/orfZ*, pCDFDuet™-1 and co-transformation with pET-28a(+)_*dhaB* and pCDFDuet™-1_*dhaT* constructs of *E. coli* BL21 (DE3) cells

The transformation procedure was initiated by employing a single 50 µL aliquot of chemically competent *E. coli* BL21 (DE3) cells per transformation, which was then thawed on ice. Subsequently, a 5 µL volume containing 100 ng of the respective plasmid DNA (pET-28a(+)_*orfX/orfZ* for the first aliquot, and empty pCDFDuet™-1 plasmid for the second aliquot), was added to the competent cells with gentle stirring. As a control, an aliquot was utilized that was mixed with 5 µL of MilliQ water instead of DNA, and analogous to the experimental samples, was subjected to the designated incubation times and conditions. This control allowed for the assessment of any non-specific effects that may arise during the transformation process. The resulting transformation mix was then incubated on ice for a duration of 30 minutes. Subsequently, the cells underwent a heat shock of precisely 30 seconds at 42°C, while refraining from any agitation and were immediately placed back on ice after the heat shock step. Further, an addition of 1 ml LB medium was made to the transformation mix, which was incubated horizontally on a spinning plate at a speed of 225 rpm and a temperature of 37°C for a period of 60 minutes. Upon completion of the incubation, 100 µL and 400 µL of the transformation mix was plated onto two agar plates, containing the necessary antibiotic (kanamycin for the pET-28a(+) and streptomycin for the pCDFDuet™-1 plasmid). The following step involved an overnight incubation at 37°C to facilitate bacterial growth and the development of discernible colonies. The succeeding day, two distinct colonies were selected from each petri dish and individually inoculated into 5 ml of LB media supplemented with the corresponding antibiotic. The resulting cultures were placed in a shaking incubator set at 220 rpm and maintained at a temperature of 37°C overnight. After the incubation period, 0.5 ml of the overnight cultures were mixed with 0.5 ml of glycerol (40%). These stocks were stored in a freezer at a temperature of -80°C for long-term preservation.

The same procedure was followed for the co-transformation of *E. coli* BL21 (DE3) cells with the pET-28a(+)_*dhaB* and pCDFDuet™-1_*dhaT* ligated vectors. The only difference was that, for each plasmid, 2.5 µL volume containing 50 ng were added to the aliquot. The cells underwent identical conditions, and subsequently, 100 µL and 400 µL of the transformation mix were separately plated on agar plates supplemented with both kanamycin and streptomycin antibiotics. After overnight incubation at 37°C, starting cultures were prepared by individually inoculating two distinct colonies from each petri dish into 5 ml of LB media supplemented with the corresponding antibiotic. The cultures were incubated under the same conditions (37°C, 220 rpm, overnight) and used for the preparation of glycerol stocks.

3.2.3. Protein expression of GDHt, GDHtR, and 1,3-PDDH

The BL21(DE3) strain is commonly utilized for recombinant protein production due to its designed ability of producing T7 polymerase and its lack of certain proteases. This feature enables efficient transcription of target genes under the control of the T7 promoter (Ratelade et al., 2009). The transformed *E. coli* BL21 (DE3) strains containing the pET-28a(+)_*dhaB* and pCDFDuet™-1_*dhaT* constructs, which were generated in previous studies conducted by the research group, were employed for this experimental series. Additionally, the transformed *E. coli* BL21 (DE3) strains carrying the pET-28a(+)_*orfX/orfZ* and pET-28a(+)_*dhaB*/pCDFDuet™-1_*dhaT* ligated vectors, as well as the *E. coli* strain containing the empty pCDFDuet™-1 (control) generated following the method outlined in subchapter 3.2.2, were used for the protein expression analysis.

To initiate the experimental procedure, an overnight culture was prepared by adding 5 µL of the glycerol stock containing the transformed cells into 5 mL of LB broth supplemented with 5 µL of the appropriate antibiotic (50 g x mL^{-1} stock concentration). The culture was then incubated in a shaking incubator at 37°C and 220 rpm overnight to facilitate cell growth. On the following day, the optical density at 600 nm (OD_{600}) of the overnight culture was measured to assess its growth. The OD_{600} was adjusted to 0.1 by inoculating a calculated volume of the overnight culture into 250 mL of fresh LB media along with 250 µL of the appropriate antibiotic (50 µg x mL^{-1}). The culture was grown in a shaking incubator at 220 rpm and 37°C, following the same conditions as the overnight culture. The OD_{600} was periodically monitored, approximately every 30 minutes, until it reached a value of 0.6, indicating the mid-exponential growth phase. At this point, 0.5 mM of isopropyl β-D-1-thiogalactopyranoside (IPTG) was added to induce protein expression. The culture was further cultivated in the shaking incubator at a lower temperature of 25°C and 220 rpm overnight. Subsequently, the cells were harvested by centrifugation (Sigma-Aldrich) at 4°C, 4000 rpm for 30 minutes after splitting them into 4-5 pre-weighted 50 mL Eppendorf tubes. The supernatant was discarded in accordance with GLPs, and the tubes were re-weighed to determine the dry mass of the cells. The cell pellets were stored at -20°C for future use.

3.2.3.1. SDS-PAGE for protein expression assessment

For protein expression analysis, one cell pellet per transformation (obtained from the procedure described in sub-chapter 3.2.3), was resuspended in approximately 4-6 mL of potassium phosphate 50 mM resuspension buffer with a pH 8.0, aiming for a dilution of 0.1 g of cells per mL. The resuspended cells underwent lysis via sonication in a UP400S sonicator set at an amplitude of 40 % and a cycle of 0.5, performed on ice. The sonication process was repeated for a total duration of approximately 8 minutes with 1-minute intervals, until a distinctive color and viscosity change indicated successful cell lysis. Subsequently, the lysed cell suspension was subjected to centrifugation (Sigma-Aldrich) at 4°C and 4500 rpm for 30 minutes. This resulted in the separation of the soluble fraction, which was

transferred to a separate Eppendorf tube. The insoluble fraction was resuspended in an equivalent volume of the resuspension buffer. The total protein concentration in both fractions was determined using the BioSpec-nano spectrophotometer (Shimadzu Corporation) by measuring the optical density (OD) at 280 nm.

Samples from both the soluble and insoluble fractions were prepared for Sodium dodecyl-sulfate polyacrylamide gel electrophoresis (SDS-PAGE) analysis. Specifically, 22.5 µL of each sample was mixed with 7.5 µL of 4X SDS-dye solution containing 4:1 ratio of Laemmli sample buffer to β-mercaptoethanol. The sample mixtures were subsequently heated for 10 minutes at 100°C. Then, 10 µL of the protein samples and 5 µL of Precision Plus Unstained Protein™ Standard (BIO-RAD) were loaded into a precast 4-20% Mini-PROTEAN® TGX Stain-Free protein gel (BIO-RAD). The SDS-PAGE electrophoresis was conducted at 90 V for 15 minutes, followed by 160 V for 30 minutes to allow for protein separation based on molecular weight. The resulting protein bands were visualized and analyzed using the GelDoc Go imaging system (BIO-RAD) with a light exposure of 45 seconds. To determine the expected size of the protein bands, their molecular weight was calculated using the SnapGene software (© 2023 SnapGene).

3.2.4. Immobilized metal affinity chromatography (IMAC) purification of GDHt and GDHtR

The cell pellets obtained from the dhaB and orfX/orfZ protein expression cultures, as described in subchapter 3.2.3, were utilized for protein purification using the immobilized metal affinity chromatography (IMAC) technique. IMAC is based on the principle that metal ions immobilized on the chromatographic support material interact with the nitrogen- or oxygen-containing side chains of amino acids. Through coupling with an appropriate chelating agent, the metal ions are bound to the chromatographic support material. Transition metals including Cu^{2+}, Ni^{2+}, and Zn^{2+} were discovered to have an affinity for nitrogen-containing side chains. This characteristic has made them suitable for utilization in IMAC to selectively bind the imidazole ring of histidine residues found within peptides and proteins (Pearson, 1990; Yang et al., 1998).

The purification protocol mirrored the steps employed for SDS-PAGE protein expression analysis described in subchapter 3.2.3.1, up to the separation of the soluble and insoluble fractions. The only exception was that binding buffer (35 mM potassium phosphate buffer, 500 mM NaCl, 20 mM imidazole, pH 8) was used instead of the resuspension buffer. The purification process of the soluble fractions of the DhaB and orfX/orfZ His-tagged proteins was conducted using a 1 mL HisTrap™ High Performance column (Cytiva), which was coupled to the GE Healthcare ÄKTA™ Start chromatography system (GE Healthcare Bio-Sciences). The UNICORN™ software served as the control platform for the purification system. Specifically, the following parameters were set: a pressure limit of 0.30 MPa, a flow rate of 1.0 mL/min, and a target elution buffer (35 mM potassium phosphate buffer, 500 mM NaCl, 500 mM imidazole, pH 8) concentration of 100.0%. For the DhaB protein, fractions T6, T7, and T8 were systematically collected, while for the orfX/orfZ protein, fractions T7, T8, and T9 were collected. All fractions were eluted in the range from 3.0% to 83.0% elution buffer concentration (**Figures A3** and **A4** of the appendix). The BioSpec-nano spectrophotometer (Shimadzu Corporation) was used to determine the total protein concentration in all fractions by measuring the optical density (OD) at 280 nm. Subsequently, the first two fractions from each purification process, along with the soluble fraction of the unpurified samples, were subjected to SDS-PAGE protein analysis. The sample preparation procedure described in the subchapter 3.2.3.1 was meticulously followed for this analysis.

3.2.5. GDHt enzymatic activity and product formation

Accurate quantification of GDHt enzymatic activity is crucial for comprehensive characterization of the enzyme, particularly in the case of GDHt-expressing whole-cell biocatalysts employed in the synthesis of substances like 1,3-PDO. Various assays can be employed to measure GDHt activity, including the colorimetric assay using 3-methyl-2-benzothiazolinone hydrazone (MBTH). An alternative method is the coupled-enzymatic conversion of aldehydes, such as 1,3-propionaldehyde, to their corresponding alcohols (1,3-PDO). This coupled reaction involves the consumption of NADH and can be easily monitored over time using spectrophotometry (Sankaranarayanan et al., 2017).

3.2.5.1. 3-methyl-2-benzothialzolinone hydrazone (MBTH) method for GDHt activity determination

The 3-methyl-2-benzothialzolinone hydrazone (MBTH) technique was used in this project to measure the activity of GDHt enzyme and to assess whether the GDHt's reactivase enzyme has an effect on this activity. The experimental methodology employed followed the protocol outlined by Daniel et al., in their publication in 1998 (Daniel et al., 1998).

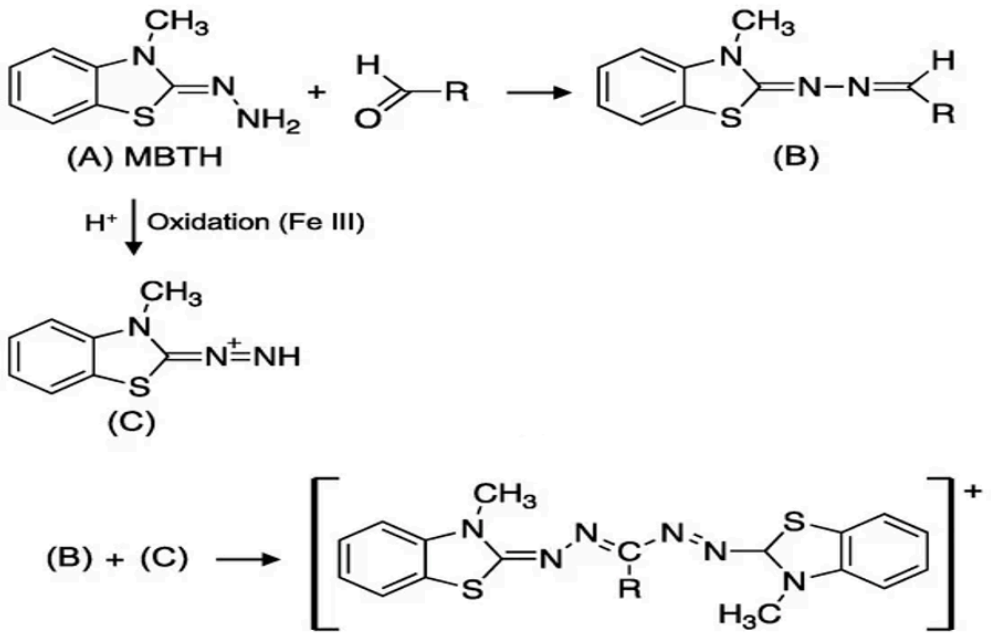

Figure 3.1: Mechanism of the 3-methyl-2-benzothiazolone hydrazone (MBTH) reaction. Where A is the MBTH compound, B the produced azine, C the reactive MBTH cation and D the blue MBTH cation product (Adapted from Dator et al., 2019).

The fundamental principle underlying this technique is that the aldehydes produced during the GDHt reaction, react with MBTH to form azine compounds. Simultaneously, MBTH undergoes oxidation, leading to the generation of a reactive cation. This reactive cation subsequently reacts with the produced azine compounds, leading to the formation of a blue-colored cation that can be detected spectrophotometrically (**Figure 3.1**) (Toraya et al., 1977; Daniel et al., 1998). Applications of the MBTH approach include kinetic and mechanistic studies, as well as the identification of substrate and cofactor specificities (Toraya et al., 1977; Daniel et al., 1998).

The MBTH method was conducted twice. Firstly, using the crude cell lysate soluble and insoluble fraction from the protein expression analysis of GDHt (*dhaB*) and/or GDHtR (*orfX/orfZ*) (subchapter 3.2.3.1) and secondly using the purified GDHt and/or GDHtR enzyme fractions T7 and T8, respectively (subchapter 3.2.4). For this purpose, four distinct reaction mixtures were prepared for each case: two without the reactivase enzyme and two with it, in a total volume of 1 mL each. An appropriate amount of GDHt enzyme and/or GDHtR was added to achieve a target concentration of approximately 0.1 μg × mL^{-1} each. Apart from the enzymes, the reaction mixtures consisted of 0.2 M 1,2-propanediol substrate, 0.05 M KCl, 15 mM coenzyme B12, and 0.035 M potassium phosphate buffer (pH 8.0). Four different controls were also prepared, lacking either 1,2-propanediol, coenzyme B12, the enzyme (in the case of purified protein), or the gene insert in the pCDFDuet™-1 vector (when using the cell lysate). Following the preparation of the assay mixtures, they were incubated at 37°C with continuous shaking at 220 rpm for 10 minutes. Then, the enzymatic reaction was terminated by adding 1 mL of 0.1 M potassium citrate buffer (pH 3.6) and 0.5 mL of MBTH hydrochloride. The resulting mixtures were further incubated under the same conditions as before and the amount of propionaldehyde generated was determined by measuring the absorbance at 305 nm. To account for any background absorbance or color contribution from the reaction components other than the enzymatic reaction itself, a blank control without the enzyme was prepared. The activity calculations were conducted utilizing the apparent molar extinction coefficient at 305 nm for the colorful product generated from 3-HPA, 13.3×10^3 $M^{-1} \times cm^{-1}$. The amount of GDHt needed to convert 1 mol of 1,2-propanediol into 3-HPA (product) in 1 min was used to define one unit (U) of enzyme activity. The detailed calculations can be found in the Appendix.

3.2.5.2. Coupled-enzymatic-reaction transformation of glycerol into 1,3-PDO

In accordance with previous research conducted by the group (DSP), it has been proven that the crude cell lysate containing the 1,3-PDDH enzyme exhibited specific activity by effectively converting propionaldehyde substrate into 1-propanol. Therefore, the 1,3-PDDH enzyme was utilized in a coupled reaction with GDHt to validate the activity of GDHt and to prove the formation of the 1,3-PDO product. The experimental approach followed was based on the method described by Sankaranarayanan et al. (2017), with some adjustments (Sankaranarayanan et al., 2017).

As stated in chapter 1.4 of the background, the GDHt enzyme, first converts glycerol to aldehyde (3-HPA) which is further transformed into alcohol (1,3-PDO) through the reduced NADH-dependent 1,3-PDDH enzyme. In the absence of GDHt activity, there would be no production of 3-HPA, resulting in the substrate unavailability for the 1,3-PDDH enzyme. Consequently, the 1,3-PDDH enzyme would remain inactive, leading to the non-consumption of the NADH cofactor. The coupled-enzymatic-reaction approach relies on monitoring this NADH cofactor consumption, during the conversion of aldehyde to alcohol, as the reaction progresses. Spectrophotometry allows for the measurement of NADH levels in a time-dependent manner, providing a means to assess the activity of the coupled reaction (Kim et al., 2016).

Similar to the MBTH method, the coupled-enzymatic-reaction approach was conducted two times. In the first case, the crude cell lysate soluble and/or insoluble fraction from the protein expression of *dhaT* (as described in subchapter 3.3.3.1) was utilized as the 1,3-PDDH enzyme source. When it comes to the GDHt enzyme, the purified fraction T7 was employed, which was obtained through the IMAC procedure outlined in subchapter 3.3.4. This involved isolating and purifying the GDHt enzyme to obtain a more refined and concentrated enzyme sample. Regarding the second case, the soluble and insoluble fractions of the cells co-expressing *dhaB* and *dhaT*, also obtained through the procedure described in subchapter 3.3.4 were employed. Initially, the substrate-cofactor mixture, which consisted

of 35 mM potassium phosphate buffer (pH 8.0, filter sterilized), 10 mM glycerol, 0.015 mM coenzyme B12 and 0.15 mM NADH was carefully transferred into a spectrophotometer cuvette with a path length of 1 cm. Following, the two enzymes were added on the reaction mix. In the first case, the coupling enzyme 1,3-PDDH was introduced in an appropriate amount to achieve a concentration of 0.05 μg x mL^{-1}. To initiate the enzymatic reaction, the GDHt enzyme was also added at a concentration of 0.05 μg × mL^{-1} and the total volume of the completely constituted reaction mixture was kept at 1 ml. In the second case, the crude cell lysate soluble fraction containing both enzymes, was added in an appropriate amount to achieve a final concentration of approximately 0.1 μg × mL^{-1} per enzyme. Different standards were also prepared, lacking either glycerol substrate, coenzyme B12, coenzyme NADH. Additionally, in the assay conducted with purified proteins, a control without the enzyme was included, while in the assay with crude cell lysate, the pCDFDuet™-1 vector without an insert served as the fourth standard. The reaction was monitored for a duration of 5 minutes using an Evolution™ 300 UV-Vis Spectrophotometer (Thermo Scientific) equipped with temperature control set at 37 °C. To establish a baseline, a reaction mixture without the NADH cofactor was used as a blank. The spectrophotometer allowed for continuous measurement of the absorbance or changes in absorbance during the enzymatic reaction over the specified time period. In order to validate product formation, the concentration of 1,3-PDO was measured using an AS-4150/4250 R High-Performance Liquid Chromatography (HPLC) system with RI-4030 refractive index detector. For the analysis, an Aminex® HPX-87H long organic acid column (BIO-RAD) was employed. The HPLC system operated at a flow rate of 0.4 mL × min^{-1}, and each sample underwent an analytical time of 40 minutes. The column's temperature was adjusted at 65°C, with the maximum pressure set at 700 bar and the minimum pressure at 3 bar. The samples were prepared for the HPLC analysis by adding 20 μL of 10% H_2SO_4 per 1 mL of sample. Subsequently, they were filtered using a syringe filter with a pore size of 0.2 μm, in order to remove any particulate matter or contaminants that may interfere with the HPLC analysis and contaminate the column. Thus, ensuring the accuracy and reliability of the results.

3.3. Introduction of GDHtR (*orfX/orfZ*) in *E. coli*

In summary, the duet expression vector pCDFDuet™-1, containing two multiple cloning sites (MCS-1 and MCS-2) for the ligation of two different inserts, was utilized in this study. The vector incorporates a noncleavable N-terminal 6xHis tag to the recombinant protein encoded by the gene inserted into MCS-1, while an S-tag is added to the expression product of the insert ligated into the MCS-2 position. In a previous study conducted by the group, the vector was ligated with the *dhaT* gene, which encodes the 1,3-PDDH protein, into the MCS-2 position. In the current work, the *orfX*/*orfZ* genes, encoding the GDHtR, were ligated into the MCS-1 position of another empty pCDFDuet™-1 vector using the Gibson Assembly method. The resulting plasmid, pCDFDuet™-1_*orfX/orfZ*, was used to transform *E. coli* DH5a competent cells that were then cultured overnight at 37°C on agar plates containing streptomycin (50 μg x mL^{-1}) as a selection marker. Lastly, colony PCR analysis was performed to confirm the success of the transformation and presence of the desired plasmid construct in the selected colonies.

3.3.1. Ligation of *orfX/orfZ* gene into pCDFDuet™-1 plasmid

The Gibson assembly method was employed for the purpose of ligating the *orfX/orfZ* genes coding for the GDHtR into the pCDFDuet™-1 vector. The experimental protocol followed the guidelines provided by New England Biolabs (NEB, 2022). Gibson et al. (2009) define the Gibson assembly as an isothermal, single-reaction approach for building numerous overlapping DNA molecules through the coordinated activity of a 5′ exonuclease, a DNA polymerase, and a DNA ligase. Prior to being

covalently linked, DNA pieces are first receded, producing single-stranded DNA overhangs that specifically anneal (Gibson et al., 2009).

To generate DNA fragments with specific overhangs that would be later used for the Gibson assembly method, a polymerase chain reaction (PCR) was utilized. The PCR reaction mixture consisted of 10 µL of Phusion™ High-Fidelity buffer (5X, containing 7.5 mM $MgCl_2$), 1 µL of dNTP mix (10 mM each), 0.5 µL of Duet_*orfX/orfZ* forward primer (10 µmol × L^{-1}, **Table A1**), 0.5 µL of Duet_*orfX/orfZ* reverse primer (10 µmol × L^{-1}, **Table A1**), 10 µL of Phusion™ High-Fidelity DNA Polymerase (2 U/µL), and 1 µL of the purified pET-28a(+)_*orfX/orfZ* ligated vector as the template. The remaining volume was adjusted with MilliQ water to a final volume of 50 µL. The primers were designed specifically to amplify the *orfX/orfZ* insert. The PCR was carried out using the thermocycling conditions as outlined in **Table 3.3**. Subsequently, a second PCR was performed, for the linearization and amplification of the pCDFDuet™-1 vector, using a similar master mix composition, with the exception of using Duet forward (10 µmol × L^{-1}, **Table A1**) and Duet reverse primers (10 µmol × L^{-1}, **Table A1**), that bind inside the vectors' MCS-1 region, and the pCDFDuet™-1 vector as the template. Variations in the thermocycling conditions for this second PCR are also detailed in **Table 3.3**. Notably, in order to evaluate the optimal annealing temperature for vector amplification, a temperature gradient ranging from 60.6°C to 66.4°C was employed. Specifically, the following temperatures were tested: 60.6°C, 61.6°C, 63.1°C, 64.9°C, and 66.4°C. To serve as a negative control, a reaction mix consisting of 1 µL MilliQ water in place of the DNA template was used. This control allowed for the assessment of non-specific amplification or contamination in the absence of the target DNA template.

Table 3.3: Thermocycling conditions for the polymerase chain reaction (PCR) amplification of the orfX/orfZ insert and the pCDFDuet™-1 vector. The temperature (°C), running time and cycles performed are indicated.

Step	Temperature	Time	Cycles
Initial Denaturation	98°C	30 sec	1
Denaturation	98°C	10 sec	35
Annealing[2]	66.4°C (for the insert) or 60.6°C – 66.4°C (for the vector)	30 sec	
Extension[3]	72°C	2 min	
Final extension	72°C	10 min	1
Hold	4°C	∞	∞

The PCR products obtained were analyzed using 1.0% analytical agarose gel electrophoresis with 1X TAE running buffer. The gel was run at a voltage of 90 V for 45 minutes. DNA Gel Loading Dye (6X) (Thermo Scientific) was used as a fluorescent dye for visualization of the DNA bands and the GeneRuler 1 kb DNA ladder (0.5 µg × mL^{-1}) (Thermo Scientific) as a molecular weight marker. Subsequently, the specific bands corresponding to the desired PCR products were cut from the gel and the QIAquick® Gel Extraction Kit (50) (QIAGEN) was employed for their purification. The purification process involved binding the PCR products to the purification column, washing away impurities, and eluting the purified DNA with a volume of 20 µL MilliQ water. The concentration of the purified DNA was determined using a BioSpec-nano spectrophotometer (Shimadzu Corporation) by measuring the absorbance at 260 nm.

[2] The annealing temperature should be 3°C higher than the lower primer Tm (New England Biolabs).
[3] For the extension time, it is recommended to use 15-30 sec per kb (New England Biolabs).

For the Gibson assembly reaction, the insert (*orfX/orfZ* genes) and the vector (pCDFDuet™-1) were combined in a 3:1 DNA molar ratio, respectively. The NEBioCalculator® tool (NEB) was used to calculate the precise amount of vector and insert needed based on their respective sizes and concentrations. In addition to the insert and vector, the reaction mix contained 10 µL NEBuilder® HiFi DNA Assembly Master Mix (NEB) and the remaining volume was adjusted with MilliQ water to a final volume of 20 µL. This master mix contained the necessary enzymes, such as a 5' exonuclease, DNA polymerase, and DNA ligase, to facilitate the assembly reaction. After incubation at 50°C for 60 min, the samples were stored at -20°C for subsequent transformation.

3.3.2. *E. coli* DH5a competent cell transformation with ligated pCDFDuet™-1_*orfX/orfZ* plasmid

The transformation procedure followed in this study was similar to the one described in subchapter 3.3.2, with the only difference being the use of *E. coli* DH5a strain instead of BL21. Briefly, the procedure involved combining a 50 µL aliquot of chemically competent *E. coli* DH5a cells with a 5 µL volume containing 1 pg to 100 ng of the pCDFDuet™-1_*orfX/orfZ* plasmid DNA (or 5 µL MilliQ water for the negative control). After incubation on ice for 30 minutes, heat shock at 42°C for 30 seconds and follow-up incubation on ice, 1 ml of LB medium was added to the transformation mix, which was incubated at 225 rpm and 37°C for 60 minutes. Following the incubation, 100 µL and 400 µL of the transformation mix was plated onto two agar plates, containing kanamycin antibiotic (50 µg x mL^{-1}), and incubated overnight at 37°C.

Seven distinct colonies were selected, after carefully marking their location at the petri dishes, and individually inoculated into 12 µL sterile MilliQ water. Then, 2 µL of the dissolved colonies were used to plate in a separate marked agar plate with kanamycin, each in their respective positions. The remaining 10 µL were used to perform colony PCR. 8 µL of DreamTaq Green PCR Master Mix (2X) were added in each tube, together with 1 µL of the T7 forward primer (10 µmol × L^{-1}, **Table A1**) and 1 µL of the T7 reverse primer (10 µmol × L^{-1}, **Table A1**), up to a total volume of 20 µL. At the same time, a negative control was prepared, with MilliQ water instead of the colony. By including this control, any observed amplification signals can be accurately attributed to the presence of the target DNA in the experimental samples, ensuring the reliability and validity of the results. After spinning down the samples, the PCR was carried out using the thermocycling conditions as outlined in **Table 3.4**.

Table 3.4: Thermocycling conditions for the colony polymerase chain reaction (PCR). The temperature (°C), running time and cycles performed are indicated.

Step	Temperature	Time	Cycles
Initial (Cell) Denaturation	95 °C	5 min	1
Denaturation (DNA)	95 °C	30 sec	35
Annealing	48 °C	30 sec	
Extension	72 °C	1 min	
Final extension	72 °C	15 min	1
Hold	4 °C	∞	∞

The PCR products were analyzed using 1.0 % agarose gel electrophoresis with 1X TAE running buffer (Acetic acid 1M, Tris base 2M, EDTA disodium salt dihydrate 50 mM), running at a voltage of 90 V for 45 minutes. The samples were loaded onto the gel without the addition of loading dye, as the DreamTaq buffer used in the PCR already contains it. The GeneRuler 1 kb DNA ladder (0.5 µg × mL^{-1}) (Thermo Scientific) as a molecular weight marker.

4. Results and Discussion

4.1. Introduction and Expression of GDHt (*dhaB*), GDHtR (*orfX/orfZ*), 1,3-PDDH (*dhaT*) in *E. coli*

The expression products of various transformed *E. coli* BL21 (DE3) strains, under the control of the T7 RNA polymerase promoter, were analyzed using SDS-PAGE electrophoresis, the results of which and their corresponding analyses are presented in this chapter. The strains included those carrying the pET-28a(+)_*dhaB*, pET-28a(+)_*orfX/orfZ*, and pCDFDuet™-1_*dhaT* constructs, as well as the strains carrying both the pET-28a(+)_*dhaB* and the pCDFDuet™-1_*dhaT* ligated vectors.

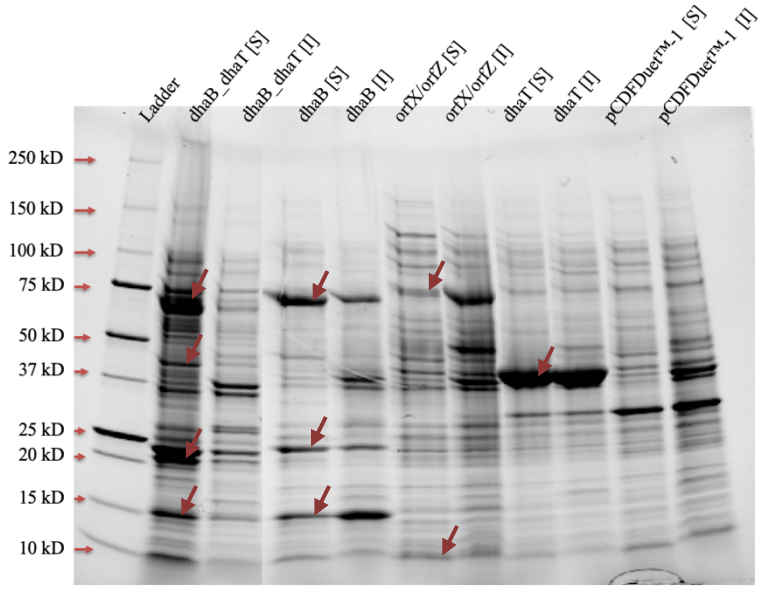

Figure 4.1: SDS-PAGE analysis of GDHt (dhaB), GDHtR (orfX/orfZ), and 1,3-PDDH (dhaT) protein expression samples. The insoluble (I) and soluble (S) fractions of recombinant E. coli BL21 (DE3) crude cell extract were run on a 4-20% Mini-PROTEAN® TGX Stain-Free™ Gel with Precision Plus Protein™ unstained ladder as the molecular weight standard. Red arrows indicate the migration positions of the different protein subunits. The GDHt protein consist of three subunits with molecular weights of 60.7 kDa, 21.3 kDa, and 16.1 kDa. The GDHtR protein is composed of two subunits with molecular weights of 63.6 kDa and 12.0 kDa. The 1,3-PDDH protein consists of a single subunit with a molecular weight of 41.4 kDa.

Figure 4.1 presents the results of SDS-PAGE analysis confirming the protein expression of *dhaB*, *orfX/orfZ*, and *dhaT*, along with the co-expression of *dhaB* and *dhaT*. Specifically, the GDHt protein was identified as three distinct bands with molecular weights of 60.7 kDa, 21.3 kDa, and 16.1 kDa, in columns 4 and 5 of the gel image. These findings are fairly consistent with the molecular weights of *Klebsiella pneumonias*' three protein subunits as determined by the Expasy – ProtParam software (SIB) analysis. It is noteworthy that the intensity of these bands revealed higher expression levels of the two larger subunits in the soluble (S) fraction compared to the insoluble (I) fraction, while the smaller subunit exhibited the opposite trend. This finding suggests differential solubility and expression patterns among the three GDHt subunits. Regarding the GDHtR protein, it consists of two subunits with molecular weights of 63.6 kDa and 12.0 kDa, which were both identified in lanes 6 and 7 of the gel

image. Higher expression is observed in the insoluble fraction compared to the soluble one. The observed high presence of proteins in the insoluble fraction could be attributed to the formation of inclusion bodies, which can occur due to various factors, including the cultivation conditions (i.e., temperature and pH) (Strandberg & Enfors, 1991; Przystałowska et al., 2015a) Additionally, the 1,3-PDDH protein consists of one subunit with molecular weight of 41.4 kDa, which was identified in lines 8 and 9. Those bands showed higher intensity compared to the pCDFDuet™-1 control (lines 10-11) and the band intensity of the protein is equal in the soluble and insoluble fraction, indicating a comparable expression pattern. Furthermore, in the co-expression sample (columns 2-3), the three subunits of the GDHt and the single subunit of the 1,3-PDDH protein were identified. These bands exhibited a higher presence in the soluble fraction compared to the insoluble fraction.

4.1.1. Immobilized metal affinity chromatography (IMAC) purification of GDHt and GDHtR

Recombinant *E. coli* BL21 (DE3) strains containing pET-28a(+)_*dhaB*, pET-28a(+)_*orfX/orfZ* vectors, were utilized for protein purification with the immobilized metal affinity chromatography (IMAC) technique. The pET-28a(+) vector was selected for its ability to incorporate a His_6-tag at the C-terminal of the target protein, facilitating purification. A 1 mL HisTrap™ High Performance column (Cytiva) was utilized for this purpose. The column was packed with highly cross-linked agarose beads attached with a nickel-charged chelating group. Only proteins with exposed histidine groups were retained by the nickel-precharged chelating group, allowing for their efficient purification.

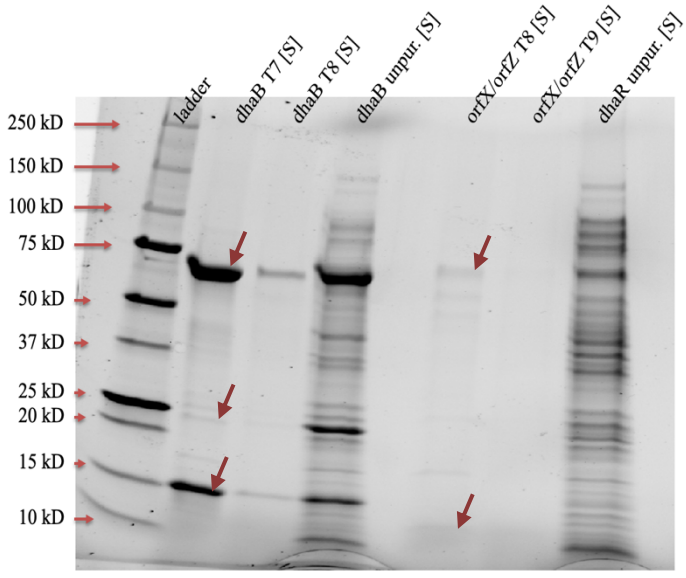

Figure 4.2: SDS-PAGE analysis of glycerol dehydratase GDHt (dhaB), and glycerol dehydratase reactivase GDHtR (orfX/orfZ) purified fractions, collected using immobilized metal affinity chromatography (IMAC). The soluble (S) fractions of recombinant E. coli BL21 crude cell extract were used for the purification and run, together with the unpurified soluble fractions (control), on a 4-20% Mini-PROTEAN® TGX Stain-Free™ Gel. Precision Plus Protein™ unstained ladder was used as the molecular weight standard). Red arrows indicate the migration positions of the different protein subunits.

In **Figure 4.2**, the results of the SDS-PAGE analysis conducted on the purified GDHt and GDHtR protein samples are illustrated. Specifically, the three subunits of the GDHt protein with molecular weights of 60.7 kDa, 21.3 kDa, and 16.1 kDa were identified in the T7 fraction (lane 2), which was eluted at a gradient[4] ranging from 42% to 63%. It is noteworthy that the band corresponding to the medium-sized subunit exhibited lower intensity compared to the other two subunits and the unpurified control. This observation could suggest that the medium-sized subunit may have a lower stability compared to the other subunits, potentially resulting in decreased protein levels during the purification process. However, these results are inconsistent the findings reported by Wang et al. in 2007. In their study, the α, β, and γ subunits of glycerol dehydratase were co-expressed, with a His_6-tag, in *E. coli* BL21. The expressed glycerol dehydratase constituted 36.1% of the total proteins, with each subunit accounting for 18.6% (α), 10.3% (β), and 7.2% (γ) of the total protein content (Wang et al., 2007).

Regarding the GDHtR protein, the SDS-PAGE analysis revealed the presence of its two subunits (63.6 kDa and 12.0 kDa) in the T8 fraction (lane 5), which was eluted at a gradient ranging from 41% to 63%. However, the band intensity of the GDHtR protein was noticeably faint compared to both the unpurified GDHtR control and the GDHt protein. One possible explanation for this observation is that the GDHtR protein eluted earlier in the purification process, potentially due to differences in the binding affinity between the protein and the Ni Sepharose High Performance affinity resin. This hypothesis is supported by the fact that the T6 fraction of the GDHt protein started eluting at a lower gradient[4] concentration of 21%. To gain further insights, it is suggested to analyze the fraction that eluted prior (range between 21% to 41%) using SDS-PAGE, which may provide additional information about the protein elution profile and the presence of impurities.

[4] The gradient refers to the gradual increase in the percentage of the elution buffer in the mobile phase, used to disrupt the specific binding interactions and facilitate the release of target molecules in affinity chromatography. A gradient of 42% means that the elution buffer constitutes 42% of the total mobile phase composition.

4.1.2. GDHt enzymatic activity and product formation

4.1.2.1. 3-methyl-2-benzothialzolinone hydrazone (MBTH) method for GDHt activity determination

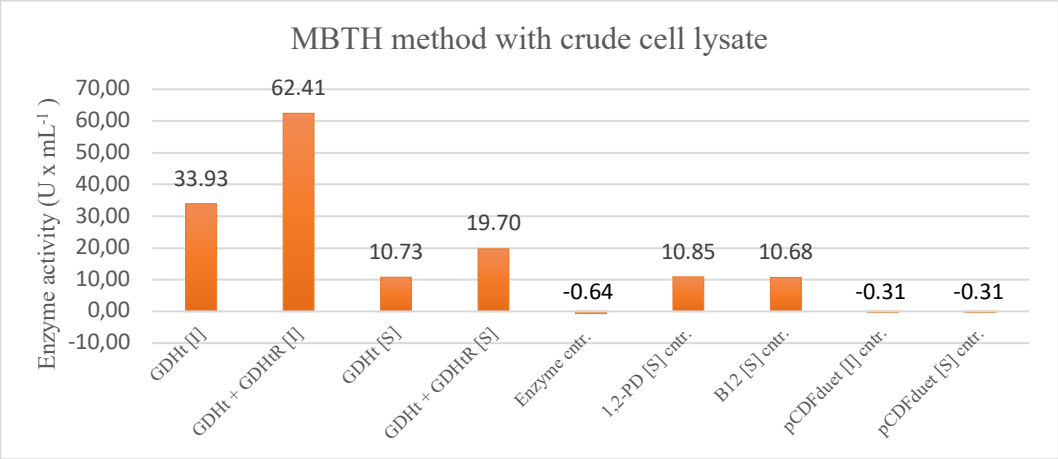

Figure 4.3: 3-methyl-2-benzothialzolinone (MBTH) activity assay results using crude cell lysate soluble (S) and insoluble (I) fractions containing glycerol dehydratase (GDHt) and glycerol dehydratase reactivase (GDHtR) proteins. The x-axis represents the samples and controls (cntr.) names, including GDHt with and without GDHtR, both in soluble and insoluble fractions, as well as 5 control samples: without enzyme, without 1,2-Propanediol, without cofactor B12, and with the empty pCDFDuet™-1 vector in both soluble and insoluble fractions. Each reaction has been performed once. The y-axis represents the enzyme activity (U ×mL-1). 1 unit (U) of enzyme activity was defined as the quantity of GDHt enzyme needed to convert 1 mol of 1,2-propanediol into propionaldehyde per minute. A blank sample, devoid of enzymes, was used to establish a baseline for the spectrophotometer.

Figure 4.3 presents the results of the MBTH method, showcasing a column chart. The chart illustrates the enzyme activity measured in U × mL^{-1} using the crude cell lysate soluble (S) and insoluble (I) fractions from the protein expression analysis of GDHt (*dhaB*) and/or GDHtR (*orfX/orfZ*).

The results revealed a noticeable variation in enzymatic activity between the soluble and insoluble fractions, regardless of the presence or absence of the GDHtR enzyme. Specifically, the enzymatic activity exhibited a lower magnitude in the soluble fraction compared to the insoluble fraction, while the values obtained for the soluble fraction were found to be comparable to the control samples lacking substrate and cofactor. The observed contrast was unexpected since there is a higher abundance of the enzyme in the soluble fraction compared to the insoluble, as verified by the SDS-PAGE analysis. Additionally, the enzyme present in the insoluble fraction primarily exists in the form of inclusion bodies or protein aggregates, which might account for the diminished enzymatic activity. Moreover, a significant increase in activity was observed in the presence of the GDHtR enzyme, regardless of the fraction. This finding underscores the vital role of the reactivase enzyme in facilitating optimal functionality of GDHt.

However, according to Sankaranarayanan et al. (2017), it is important to consider that crude cell extracts may contain aldehydes or metabolites that can react with MBTH or tryptophan, leading to potential interference with the observed absorbance. Particularly, the 3-HPA produced by GDHt can interact with other cellular elements or undergo further conversion by enzymes like oxidoreductases and/or aldehyde dehydrogenases before reacting with MBTH or tryptophan (Sankaranarayanan et al., 2017). Therefore,

the results obtained cannot be solely attributed to the activity of GDHt alone. The results of the purified GDHt enzyme would provide a more accurate estimation of its' activity. Furthermore, it should be noted that the lack of duplicate assays, which was a result of the unavailability of the corresponding enzymes, prevents the characterization of these results as statistically significant.

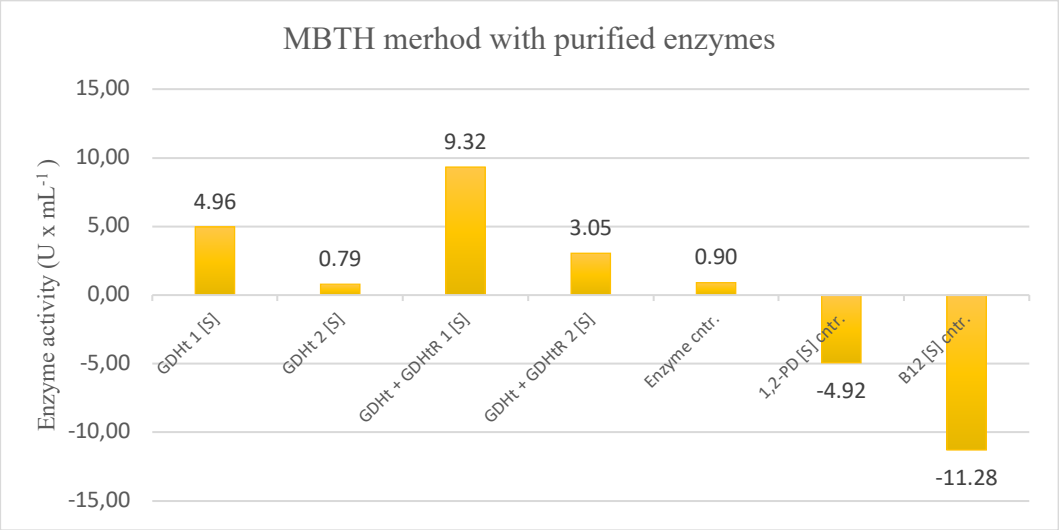

Figure 4.4: 3-methyl-2-benzothialzolinone (MBTH) activity assay results using purified glycerol dehydratase (GDHt) and glycerol dehydratase reactivase (GDHtR) enzymes, derived from the soluble (S) fraction of crude cell extract after IMAC purification.. The x-axis represents the samples and controls (cntr.) names, including GDHt with and without GDHtR, performed in duplicates, as well as three control samples: without enzyme, without 1,2-Propanediol, and without cofactor B12. The y-axis represents the enzyme activity ($U \times mL^{-1}$). 1 unit (U) of enzyme activity was defined as the quantity of GDHt enzyme needed to convert 1 mol of 1,2-propanediol into propionaldehyde per minute. A blank sample, devoid of enzymes, was used to establish a baseline for the spectrophotometer.

Figure 4.4 illustrates the results of the second MBTH method, which was conducted using the purified GDHt and/or GDHtR enzymes obtained from the soluble fraction (S) of the protein expression analysis.

As observed in the graph, there is a noticeable difference in the activity values between the duplicate samples. Specifically, in the case of the plain GDHt enzyme, the activity value obtained is similar to that of the control sample without enzyme. One possible explanation for this inconsistency could be that the enzyme concentration varied among the duplicate samples, which could have significantly influenced the enzymatic activity. It is plausible that the formation of precipitates, which were observed in the enzyme solution during its storage in the elution buffer (35 mM potassium phosphate buffer, 500 mM NaCl, 500 mM imidazole, pH 8), could have impacted the concentration of the enzyme within the sample. This occurrence of precipitation may have consequently led to a reduction in enzymatic activity due to the diminished availability of the enzyme in the solution but also due to its' inactivation. Moreover, it is worth noting that the control sample without cofactor B12 displayed a notably low enzymatic activity. This observation raises the possibility that the cofactor may have an influence on the assay, as the absorbance measurements used for calculating the activity values may be affected by the cofactor's absorbance at similar wavelengths.

4.1.2.2. Coupled-enzymatic-reaction transformation of glycerol into 1,3-PDO

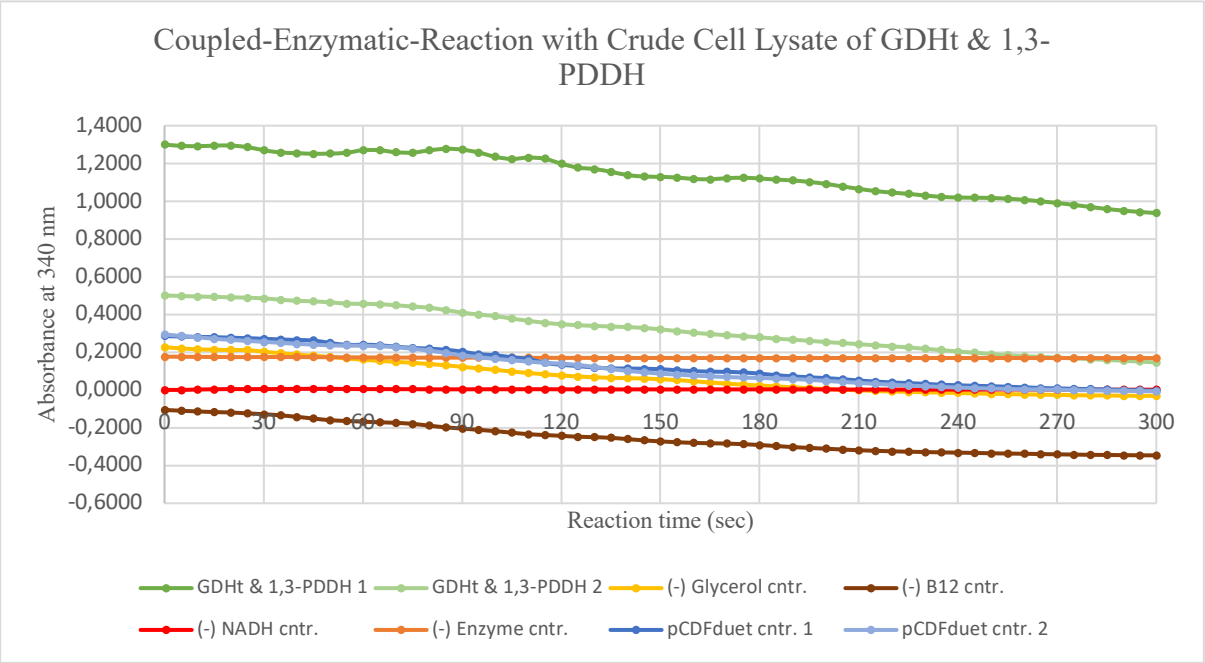

Figure 4.5: Coupled-enzyme activity assay results by monitoring the consumption of NADH coenzyme of 1,3-PDDH. Crude cell lysate soluble (S) fraction containing glycerol dehydratase (GDHt) and 1,3-propanediol dehydrogenase (1,3-PDDH) proteins was used for the assay. The x-axis represents the reaction time in seconds while the y-axis the absorbance values at 340 nm. A blank sample, devoid of NADH, was used to establish a baseline for the spectrophotometer. The reaction progress was monitored for a duration of 5 minutes. The line chart displays the various samples using distinct colors, including GDHt with 1,3-PDDH reaction samples (green and light green). Additionally, five control samples were included: without glycerol (yellow), without B12 cofactor (brown), without NADH cofactor (red), without enzyme (orange), and with the empty pCDFDuet™-1 vector in the soluble fraction (blue and light blue). A blank sample, devoid of NADH, was included in the experiment to establish a baseline for the spectrophotometer.

The results presented in **Figure 4.5** demonstrate the alterations in NADH concentration during the coupled-enzymatic transformation of glycerol to 1,3-PDO, depicted as a line chart. The coupled-enzymatic-reaction approach relies on monitoring the consumption of the NADH cofactor at 340 nm during the conversion of 3-HPA to 1,3-PDO, catalyzed by the 1,3-PDDH enzyme. Crude cell lysate soluble (S) fractions derived from *E. coli* BL21 (DE5) cells coexpressing GDHt (*dhaB*) and 1,3-PDDH (*dhaT*) were employed in this assay.

The experimental results demonstrate that the control without the addition of crude cell extract, and hence the enzymes, was the only sample that displayed a consistent absorbance value at 340 nm throughout the assay, indicating a stable NADH concentration. In contrast, all other samples, including the pCDFDuet™-1 control, exhibited a gradual decrease in absorbance, suggesting a decline in NADH concentration. Although, the observed decline in absorbance cannot be solely attributed to the coupled-enzymatic reaction responsible for the conversion of glycerol to 3-HPA and subsequently to 1,3-PDO. Firstly, the control sample lacking cofactor B12 displayed negative absorbance values, which progressively decreased over time. This suggests that vitamin B12, present in all other samples, may also absorb light at 340 nm. This finding is consistent with the work of Zheng and Lu (1996), who reported an increase in absorbance starting around 320 nm and reaching a peak at 361 nm for vitamin B12 in solutions with pH 7 or higher (Zheng and Lu, 1996). Furthermore, the initial absorbance values varied among samples, despite the addition of the same quantity of NADH in the assay mix. This

discrepancy suggests the presence of other compounds in the crude cell extracts that absorb light at the same wavelength or intracellular NADH. Moreover, the decrease in NADH concentration observed in all samples containing cell lysate, and especially the pCDFDuet™-1 control that didn't contain any enzyme, can be attributed to the activity of various cellular enzymes, including oxidoreductases, aldehyde dehydrogenases, and components of the electron transport chain. These enzymes may consume or generate NADH, potentially influencing the assay reactions and affecting the accurate measurement of GDHt activity (Kim et al., 2016).

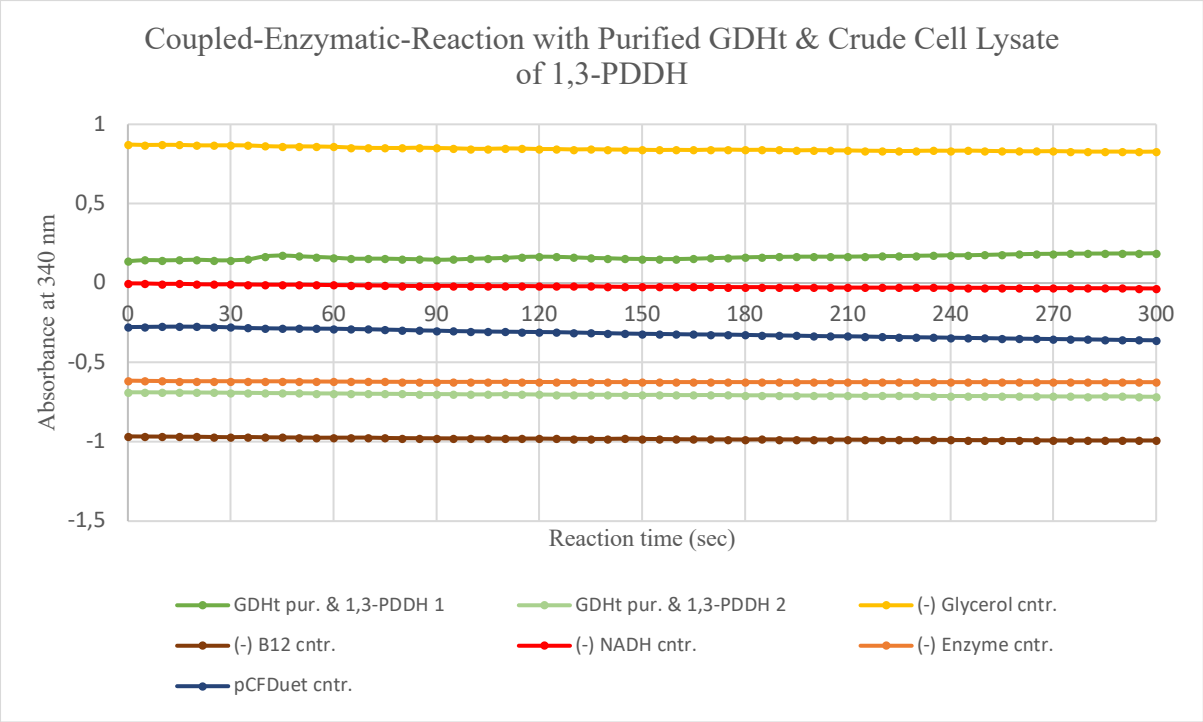

Figure 4.6: Coupled-enzyme activity assay results by monitoring the consumption of NADH coenzyme of 1,3-PDDH. Purified (pur.) glycerol dehydratase (GDHt) enzyme and crude cell lysate soluble (S) fraction containing 1,3-propanediol dehydrogenase (1,3-PDDH) were used for the assay. The x-axis represents the reaction time in seconds while the y-axis the absorbance values at 340 nm. The reaction progress was monitored for a duration of 5 minutes. The line chart displays the various samples using distinct colors, including GDHt with 1,3-PDDH reaction samples (green and light green). Additionally, five control samples were included: without glycerol (yellow), without B12 cofactor (brown), without NADH cofactor (red), without enzyme (orange), and with the empty pCDFDuet™-1 vector in the soluble fraction (blue). A blank sample, devoid of NADH, was included in the experiment to establish a baseline for the spectrophotometer.

Figure 4.6 illustrates the results of the second coupled-enzymatic transformation, aiming to convert glycerol to 1,3-PDO. The experiment involved the utilization of purified GDHt enzyme and the crude cell lysate soluble (S) fraction obtained from the protein expression analysis of 1,3-PDDH (*dhaT*).

The experimental results revealed a distinct trend compared to **Figure 4.5**. In this case, the absorbance values for all samples and controls remained constant throughout the assay, indicating a lack of significant changes in the NADH concentration. However, it is noteworthy that the initial absorbance values varied among the samples, despite the addition of the same quantity of NADH in the assay mixture. Only the sample 1, which included both enzymes, and the control without glycerol displayed positive absorbance values. The absorbance of the NADH control remained consistently at zero, while the remaining samples exhibited negative absorbance values that remained constant. The observed variations in the initial absorbance values can be attributed to the presence of intracellular NADH, as

all the samples, except the enzyme control, contained crude cell extract. The constant absorbance throughout the assay contrasts with the expected slight decrease in absorbance due to the activity of other cellular enzymes, as indicated by previous results. Thus, it suggests a possible inactivation of the enzymes.

To validate the formation of 1,3-PDO product, the samples obtained from the previous assays were subjected to High-Performance Liquid Chromatography (HPLC) analysis using an RI-4030 refractive index detector. To prepare the samples for HPLC analysis, 20 µL of 10% H_2SO_4 was added per 1 mL of each sample. The acid treatment was employed to facilitate the separation and detection of the target compound. However, the results obtained from the HPLC analysis (Figures A5 and A6), revealed no detectable presence of the desired product, 1,3-PDO. Consequently, based on the absence of product detection, the activity of the enzymes involved in the conversion process could not be confirmed. The inability to detect the final product, further supports the earlier observations and claims that the reactions did not yield the desired outcome.

4.2. Introduction of GDHtR (*orfX/orfZ*) in *E. coli*

In this study, the *orfX/orfZ* genes, which encode the GDHtR enzyme, were ligated into the MCS-1 position of the pCDFDuet™-1 vector using the Gibson Assembly method. The resulting pCDFDuet™-1_*orfX/orfZ* construct was subsequently introduced into competent *E. coli* DH5a cells via transformation. To confirm the successful transformation and the presence of the desired plasmid construct, a colony PCR analysis was performed. The results of this analysis are presented in this chapter.

4.2.1. Ligation of *orfX/orfZ* gene into pCDFDuet™-1 plasmid

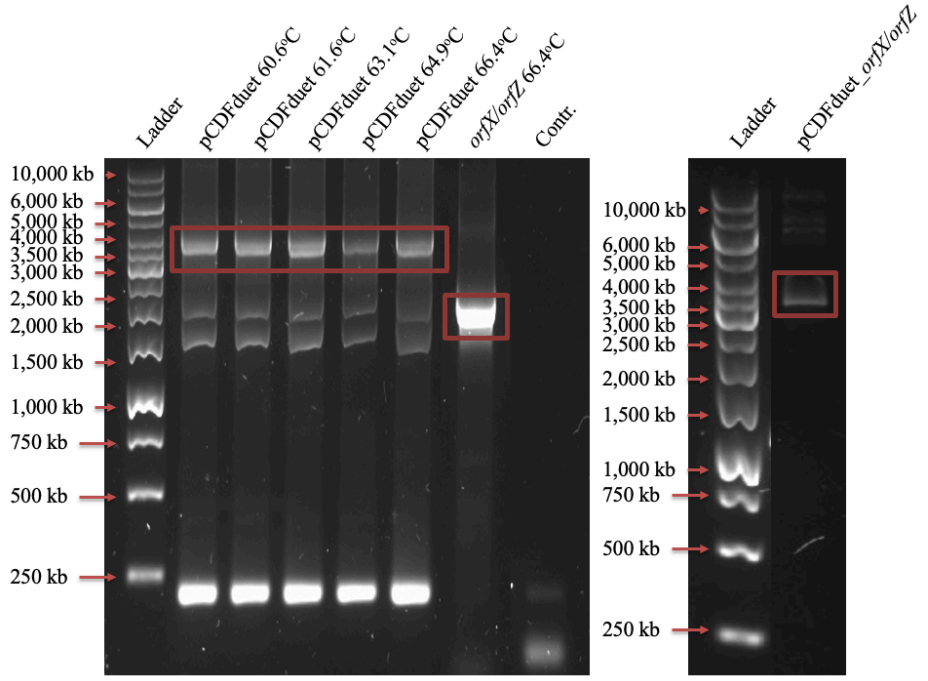

Figure 4.7: Left: Agarose gel electrophoresis of PCR amplification products. The orfX/orfZ insert and pCDFDuet™-1 vector were amplified using different annealing temperatures for subsequent use in a Gibson assembly ligation process.. Right: Agarose gel electrophoresis of the ligated pCDFDuet™-1_ orfX/orfZ construct following the Gibson assembly process. In both cases, the GeneRuler 1 kb DNA ladder (0.5 µg × mL^{-1}) (Thermo Scientific) was utilized as a size reference. The desired zones are highlighted within red squares.

In the left part of **Figure 4.7**, the agarose gel electrophoresis results of the PCR amplification process of the pCDFDuet™-1 vector (columns 2-6) and the *orfX/orfZ* insert (column 7), are presented. The objective was to amplify these DNA fragments while incorporating complementary overhangs to enable ligation through the Gibson Assembly method. For the pCDFDuet™-1 vector, different annealing temperatures (60.6°C, 61.6°C, 63.1°C, 64.9°C, and 66.4°C) were tested to determine the optimal temperature. As shown in the figure, all samples using pCDFDuet™-1 as a template (columns 2-6) exhibited four distinct bands, with the top band appearing at approximately 3,700 bp. This aligns with the expected length of 3,772 bp, as calculated using the SnapGene software (© 2023 SnapGene). Notably, the target band corresponding to the 63.1°C annealing temperature displayed slightly higher intensity compared to the other samples, indicating that this temperature was identified as the optimal condition among those tested. In addition to the desired band, a band with greater intensity and length below 250 bp was observed, which is indicative of primer-dimer formation. This phenomenon occurs

when the primers anneal to each other and amplify without binding to the target DNA template. The presence of this band in the negative control sample , which does not contain any DNA template, provides additional evidence supporting the conclusion that it is indeed a result of primer-dimer formation. Regarding the orfX/orfZ insert amplification (column 7), a single distinct band of approximately 2,000 bp was observed. This aligns with the expected length of 2,213 bp, as calculated using the SnapGene software (© 2023 SnapGene). The consistency between the experimental observation and the predicted size further supports the successful amplification of the orfX/orfZ insert during the PCR process. Moreover, the absence of any bands in the negative control sample without DNA template (column 8) reinforces the notion that there was no unintended contamination or amplification, confirming the specificity of the PCR reaction. The bands enclosed in red squares were cut from the gel and purified using the QIAquick® Gel Extraction Kit (50) (QIAGEN), to be used in the following Gibson assembly prosses.

In the right section of **Figure 4.7**, the agarose gel electrophoresis results of the Gibson assembly ligation of the pCDFDuet™-1 vector and the orfX/orfZ insert are displayed. Interestingly, an observed band with an approximate size of 3,800 bp was identified, which deviates from the anticipated band size of 5,653 bp as determined by computational analysis using the SnapGene software (© 2023 SnapGene). However, despite the deviation in size, the band of interest, marked by a red square in the figure, was cut from the gel and subjected to purification using the QIAquick® Gel Extraction Kit (50) (QIAGEN). This purification step was performed to isolate and obtain the DNA construct for subsequent transformation experiments involving *E. coli* DH5a cells.

4.2.2. *E. coli* DH5a competent cell transformation with ligated pCDFDuet™-1_*orfX/orfZ* plasmid

After an overnight incubation of the transformed cells on agar plates containing kanamycin antibiotic (50 μg x mL^{-1}), the success of the transformation was confirmed by the presence of distinct colonies. Seven colonies were selected for further analysis and subjected to colony PCR using the T7 forward and T7 reverse primer pair. The T7 forward primer has two binding sites within the pCDFDuet™-1 vector, specifically in the T7 promoters located before the MCS-1 and MCS-2 regions. On the other hand, the T7 reverse primer binds after the end of the MCS-2 region, near the T7 terminator. If the ligation process of the previous subchapter was successful, two distinct bands with lengths of 2,213 bp and 252 bp would be expected in the agarose gel electrophoresis results of the colony PCR products. The 2,213 bp band would correspond to an amplified fragment containing both the MCS-1 region where the insert is expected to be ligated and the MCS-2 region. On the other hand, the 252 bp band would correspond to an amplified fragment containing only the MCS-2 region.

However, upon analyzing the gel electrophoresis results (Figure A7, appendix), several different bands were observed, with the most intense band appearing at approximately 1,400 bp. Additionally, a band was detected in the negative control, indicating the presence of contamination. As a result, the success of the ligation experiment for incorporating the orfX/orfZ insert into the pCDFDuet™-1 vector could not be confirmed. Further investigation and optimization may be required to determine the cause of the observed bands and to validate the successful construction of the desired plasmid construct.

5. Future Prospects and Outlook

The study focused on evaluating the specific activity of the glycerol dehydratase enzyme (GDHt) in the *E. coli* BL21 (DE5) strain and investigating the impact of GDHtR on its activity. Several genes involved in 1,3-propanediol synthesis, including *dhaB* (encoding GDHt), *orfX,* and *orfZ* (for GDHt reactivase), and *dhaT* (for 1,3-propanediol dehydrogenase), were selected from *K. pneumonia*.

The MBTH method was utilized, employing crude cell lysate from *E. coli* BL21 cells as the enzyme source. Initial assessments revealed detectable activity levels for GDHt, with 10.73 U/mL in the soluble fraction and 33.93 U/mL in the insoluble fraction. Upon the addition of GDHtR, the activity levels increased to 19.70 U/mL and 62.42 U/mL, respectively, indicating the influence of GDHtR on GDHt's activity. However, it was noted that those activity values could not be solely attributed to the GDHt enzyme due to the possibility of aldehydes or metabolites present in crude cell extracts interfering with the MBTH assay and absorption measurements. Furthermore, the 3-HPA produced by GDHt can interact with other cellular components or undergo additional conversions catalyzed by oxidoreductases and/or aldehyde dehydrogenases present in the crude cell extract (Sankaranarayanan et al., 2017). Therefore, careful consideration is necessary when interpreting the results. To address these complexities, the assay was repeated using purified enzymes, but no statistically significant data were obtained under these conditions. Notably, the control sample lacking cofactor B12 exhibited significantly lower enzymatic activity, suggesting a potential influence of the cofactor on the assay. The absorption measurements at 305 nm used for activity calculations may be affected by the absorption properties of the cofactor at similar wavelengths. Therefore, additional investigations and controls focusing on the role of the B12 cofactor and its potential interference with absorbance measurements are warranted to clarify this effect. Moreover, it is recommended to repeat the MBTH method using purified enzymes and perform triplicate measurements to obtain more statistically significant data. This will enhance the reliability and accuracy of the activity calculations, enabling a comprehensive assessment of GDHt activity in the system.

The coupled-enzyme reaction was employed as another approach to validate GDHt's activity and assess the conversion of glycerol into 1,3-propanediol. In this method, GDHt and the previously validated NADH-dependent 1,3-PDDH enzyme were combined. The consumption of NADH was monitored as an indication of enzymatic activity, and HPLC analysis was performed to detect the final product. When crude cell lysate of *E. coli* BL21 cells was used as the source of both enzymes, a decrease in absorbance (OD_{340}) was observed. However, this decrease could not be solely attributed to the coupled-enzymatic reaction. Similar to the previous assay, the control sample lacking cofactor B12 exhibited negative absorbance values, suggesting that vitamin B12 may also absorb light at 340 nm. This finding aligns with the work of Zheng and Lu (1996), who reported an increase in absorbance starting around 320 nm and peaking at 361 nm for vitamin B12 in solutions with a pH of 7 or higher (Zheng and Lu, 1996). To ensure accurate and reliable measurement of GDHt activity in future studies, it is crucial to thoroughly elucidate potential interferences arising from B12 absorption. Additionally, a decrease in the absorbance was observed in the pCDFDuet™-1 control samples, containing only the crude cell extract without the enzyme. Kim et al. (2016) have highlighted challenges associated with employing crude cell extract, including the presence of cellular NADH and the activities of various cellular enzymes such as oxidoreductases, aldehyde dehydrogenases, and components of the electron transport chain, which can influence the assay reactions. These cellular components may utilize or produce NADH, potentially affecting the absorbance values and interfering with the accurate measurement of GDHt activity (Kim et al., 2016). Thus, further investigation is required to determine the extent to which the coupled-enzyme reaction can precisely gauge GDHt activity in crude cell extract.

When using purified GDHt enzyme, the crude cell extract was still included as a 1,3-PDDH source, which implies that the challenges associated with crude cell extract were not fully avoided. It is recommended to purify 1,3-PDDH and assess its activity before incorporating it into the coupled-enzyme reaction to obtain a more accurate estimation of GDHt's activity. Alternatively, commercially available enzymes such as aldehyde dehydrogenase (KGSADH) or yeast-alcohol dehydrogenase (yADH), with proven enzymatic activity, can be purchased and employed for the activity assay. Sankaranarayanan et al. (2017) utilized these enzymes in their study, as they effectively converted 1,2-propionaldehyde either to 1-propionic acid with NADH production or to 1-propanol with NADH consumption, respectively. The 1,2-propionaldehyde derived from 1,2-propanediol (1,2-PDO), which was used as an alternative substrate for GDHt (Sankaranarayanan et al., 2017). Considering that GDHt is well reported to be deactivated by glycerol and oxygen in the literature (Toraya et al., 1976; Liao et al., 2003a; Sun et al., 2003), it is recommended to use an alternative substrate such as 1,2-PDO and avoid overexposure of the GDHt enzyme to oxygen by using for example closed capped cuvettes. Lastly, in the coupled-enzyme GDHt assay, the second reaction needs to proceed significantly faster than the first reaction catalyzed by GDHt to avoid the second reaction becoming rate-determining and interfering with the measurement of GDHt's activity. Thus, saturation curves of GDHt activity with the coupling enzymes should be generated to identify the proper ratio between the two enzymes catalyzing the first and second reactions. By addressing these considerations and optimizing the experimental conditions, a more accurate assessment of GDHt's activity can be achieved in future studies.

To ensure the reliability of the integration experiments involving the *orfX* and *orfZ* genes, which code for glycerol dehydratase reactivase (GDHtR), it is recommended to repeat the ligation experiments using different thermocycling conditions for the polymerase chain reaction (PCR) process. Furthermore, for the ligation process, the pCDFDuet™-1_*dhaT* ligated vector containing the *dhaT* gene in the MCS-2 position should be employed. Subsequent verification of the integrated genes' correct orientation and accurate integration can be achieved through sequencing analysis of the resulting pCDFDuet™-1_*orfX/orfZ_dhaT* construct. Once the construct is validated, it can be transformed into *E. coli* BL21 (DE5) cells, along with the pET-28a(+)_*dhaB* plasmid that carries gene coding for GDHt. The simultaneous co-expression of all three enzymes is anticipated to facilitate the conversion of glycerol into 1,3-propanediol (1,3-PDO), according to the literature. Particularly, in a study by Wang et al. (2007), two plasmids carrying the GDHt, GDHtR, and 1,3-PDDH coding genes were utilized to genetically modify *E. coli*. All genes derived from *K. pneumoniae* and were expressed under the control of the T7 promoter. The recombinant *E. coli* strain was then subjected to fed-batch fermentation using 14.3 g/L glycerol supplemented with glucose, which resulted in the production of 8.6 g/L of 1,3-PDO. The conversion rate achieved was 0.68 mol of 1,3-PDO per mol of glycerol (Wang et al., 2007). By comparing the obtained results with the co-expression samples of GDHt and 1,3-PDDH enzymes, it will be possible to evaluate the potential contribution of the reactivation factor to the activity of GDHt.

References

Ahrens, K., Menzel, K., Zeng, A.-P., & Deckwer, W.-D. (1998). Kinetic, dynamic, and pathway studies of glycerol metabolism by *Klebsiella pneumoniae* in anaerobic continuous culture: III. enzymes and fluxes of glycerol dissimilation and 1,3-Propanediol Formation. Biotechnology and Bioengineering, 59(5), 544–552. https://doi.org/10.1002/(sici)1097-0290(19980905)59:5<544::aid-bit3>3.0.co;2-a

Arntz, D., & Wiegand, N. (1991). Method of preparing 1,3-propanediol. United States Patent 5015789.

Ashok, S., Raj, S. M., Rathnasingh, C., & Park, S. (2011). Development of recombinant *Klebsiella pneumoniae* ΔDHAT strain for the co-production of 3-hydroxypropionic acid and 1,3-propanediol from glycerol. Applied Microbiology and Biotechnology, 90(4), 1253–1265. https://doi.org/10.1007/s00253-011-3148-z

Ashurst, J. V., & Dawson, A. (2023, January). *Klebsiella pneumonia*. StatPearls - NCBI bookshelf. Retrieved May 1, 2023, from https://www.ncbi.nlm.nih.gov/books/NBK519004/

Barbirato, F., Camarasa-Claret, C., Grivet, J. P., & Bories, A. (1995). Glycerol fermentation by a new 1,3-propanediol-producing microorganism :*Enterobacter agglomerans*. Applied Microbiology and Biotechnology, 43(5), 786–793. https://doi.org/10.1007/bf02431909

Biebl, H., Menzel, K., Zeng, A.-P., & Deckwer, W.-D. (1999). Microbial production of 1,3-propanediol. Applied Microbiology and Biotechnology, 52(3), 289–297. https://doi.org/10.1007/s002530051523

Chaminand, J., Djakovitch, L., Gallezot, P., Marion, P., Pinel, C., & Rosier, C. (2004). Glycerol hydrogenolysis on heterogeneous catalysts. Green Chemistry. Retrieved April 25, 2023, from https://pubs.rsc.org/en/content/articlelanding/2004/gc/b407378a#!

Chen, L., & Hatti-Kaul, R. (2017). Exploring *Lactobacillus reuteri* DSM20016 as a biocatalyst for transformation of longer chain 1,2-diols: Limits with Microcompartment. PLOS ONE, 12(9). https://doi.org/10.1371/journal.pone.0185734

Cheng, K.-K., Zhang, J.-A., Liu, D.-H., Sun, Y., Yang, M.-D., & Xu, J.-M. (2006). Production of 1,3-propanediol by *Klebsiella pneumoniae* from glycerol broth. Biotechnology Letters, 28(22), 1817–1821. https://doi.org/10.1007/s10529-006-9158-8

Daniel, R., Bobik, T. A., & Gottschalk, G. (1998). Biochemistry of coenzyme B12-dependent glycerol and diol dehydratases and organization of the encoding genes. FEMS microbiology reviews, 22(5), 553–566. https://doi.org/10.1111/j.1574-6976.1998.tb00387.x

Daniel, R., Boenigk, R., & Gottschalk, G. (1995a). Purification of 1,3-propanediol dehydrogenase from *Citrobacter freundii* and cloning, sequencing, and overexpression of the corresponding gene in *Escherichia coli*. Journal of Bacteriology, 177(8), 2151–2156. https://doi.org/10.1128/jb.177.8.2151-2156.1995

Daniel, R., Stuertz, K., & Gottschalk, G. (1995b). Biochemical and molecular characterization of the oxidative branch of glycerol utilization by *Citrobacter Freundii*. Journal of Bacteriology, 177(15), 4392–4401. https://doi.org/10.1128/jb.177.15.4392-4401.1995

Dator, R. P., Solivio, M. J., Villalta, P. W., & Balbo, S. (2019). Bioanalytical and mass spectrometric methods for aldehyde profiling in biological fluids. Toxics, 7(2), 32. https://doi.org/10.3390/toxics7020032

Dharmadi, Y., Murarka, A., & Gonzalez, R. (2006). Anaerobic fermentation of glycerol *by Escherichia coli*: A new platform for metabolic engineering. Biotechnology and Bioengineering, 94(5), 821–829. https://doi.org/10.1002/bit.21025

Doitomi, K., Kamachi, T., Toraya, T., & Yoshizawa, K. (2012). Inactivation mechanism of glycerol dehydration by diol dehydratase from combined quantum mechanical/molecular mechanical calculations. Biochemistry, 51(45), 9202–9210. https://doi.org/10.1021/bi300488u

Forage, R. G., & Lin, E. C. (1982). DHA system mediating aerobic and anaerobic dissimilation of glycerol in *Klebsiella pneumoniae* NCIB 418. Journal of Bacteriology, 151(2), 591–599. https://doi.org/10.1128/jb.151.2.591-599.1982

Gibson, D. G., Young, L., Chuang, R.-Y., Venter, J. C., Hutchison, C. A., & Smith, H. O. (2009). Enzymatic assembly of DNA molecules up to several hundred kilobases. Nature Methods, 6(5), 343–345. https://doi.org/10.1038/nmeth.1318

Golding, B. T., & Buckel, W. (1998). Comprehensive Biological Catalysis, vol. III , pp. 239–259, Academic Press, New York, 1998

González-Pajuelo, M., Meynial-Salles, I., Mendes, F., Soucaille, P., & Vasconcelos, I. (2006). Microbial conversion of glycerol to 1,3-propanediol: Physiological comparison of a natural producer, *Clostridium butyricum* VPI 3266, and an engineered strain, *Clostridium acetobutylicum* DG1(PSPD5). Applied and Environmental Microbiology, 72(1), 96–101. https://doi.org/10.1128/aem.72.1.96-101.2006

Goodsell, D. S., & Olson, A. J. (2000). Structural symmetry and protein function. Annual Review of Biophysics and Biomolecular Structure, 29(1), 105–153. https://doi.org/10.1146/annurev.biophys.29.1.105

Gundogan, N. (2014). *Klebsiella*. Encyclopedia of Food Microbiology, 383–388. https://doi.org/10.1016/b978-0-12-384730-0.00172-5

Gutknecht, R., Beutler, R., Garcia-Alles, L. F., Baumann, U., & Erni, B. (2001). The dihydroxyacetone kinase of *Escherichia coli* utilizes a phosphoprotein instead of ATP as phosphoryl donor. The EMBO journal, 20(10), 2480–2486. https://doi.org/10.1093/emboj/20.10.2480

Han, J.-H., Batey, S., Nickson, A. A., Teichmann, S. A., & Clarke, J. (2007). The folding and evolution of multidomain proteins. Nature Reviews Molecular Cell Biology, 8(4), 319–330. https://doi.org/10.1038/nrm2144

Hansen, A. C., Zhang, Q., & Lyne, P. W. (2005). Ethanol-diesel fuel blends -- a review. Bioresource technology, 96(3), 277–285. https://doi.org/10.1016/j.biortech.2004.04.007

Honda, S., Toraya, T., & Fukui, S. (1980). In situ reactivation of glycerol-inactivated coenzyme B12-dependent enzymes, glycerol dehydratase and diol dehydratase. Journal of Bacteriology, 143(3), 1458–1465. https://doi.org/10.1128/jb.143.3.1458-1465.1980

Jiang, W., Wang, S., Wang, Y., & Fang, B. (2016). Key enzymes catalyzing glycerol to 1,3-propanediol. Biotechnology for Biofuels, 9(1). https://doi.org/10.1186/s13068-016-0473-6

Johnson, D. T., & Taconi, K. A. (2007). The glycerin glut: Options for the value-added conversion of crude glycerol resulting from biodiesel production. Environmental Progress, 26(4), 338–348. https://doi.org/10.1002/ep.10225

Johnson, E. A., & Lin, E. C. (1987). *Klebsiella pneumoniae* 1,3-propanediol:NAD^+ oxidoreductase. Journal of Bacteriology, 169(5), 2050–2054. https://doi.org/10.1128/jb.169.5.2050-2054.1987

Ju, J.-H., Heo, S.-Y., Choi, S.-W., Kim, Y.-M., Kim, M.-S., Kim, C.-H., & Oh, B.-R. (2021). Effective bioconversion of 1,3-propanediol from biodiesel-derived crude glycerol using organic acid resistance–enhanced *Lactobacillus reuteri* JH83. Bioresource Technology, 337, 125361. https://doi.org/10.1016/j.biortech.2021.125361

Jun, S.-A., Moon, C., Kang, C.-H., Kong, S. W., Sang, B.-I., & Um, Y. (2009). Microbial fed-batch production of 1,3-propanediol using raw glycerol with suspended and immobilized *Klebsiella pneumoniae*. Applied Biochemistry and Biotechnology, 161(1-8), 491–501. https://doi.org/10.1007/s12010-009-8839-x

Kim, C., Ainala, S. K., Oh, Y.-K., Jeon, B.-H., Park, S., & Kim, J. R. (2016). Metabolic flux change in *Klebsiella pneumoniae* L17 by anaerobic respiration in microbial fuel cell. Biotechnology and Bioprocess Engineering, 21(2), 250–260. https://doi.org/10.1007/s12257-015-0777-6

Kaur, G., Srivastava, A. K., & Chand, S. (2012). Advances in biotechnological production of 1,3-propanediol. Biochemical Engineering Journal, 64, 106–118. https://doi.org/10.1016/j.bej.2012.03.002

Kumar, V., Ashok, S., & Park, S. (2013). Recent advances in biological production of 3-hydroxypropionic acid. Biotechnology Advances, 31(6), 945–961. https://doi.org/10.1016/j.biotechadv.2013.02.008

Kumar, V., & Park, S. (2018). Potential and limitations of *Klebsiella pneumoniae* as a microbial cell factory utilizing glycerol as the carbon source. Biotechnology Advances, 36(1), 150–167. https://doi.org/10.1016/j.biotechadv.2017.10.004

Kurian, J. V. (2005). A new polymer platform for the future — Sorona® from corn derived 1,3-propanediol. Journal of Polymers and the Environment, 13(2), 159–167. https://doi.org/10.1007/s10924-005-2947-7

Lam, K.T., Powell, J.B., & Weider, P.R. (1997). Process for preparing 1,3- propanediol. United states patent WO1997016250 A1.

Liao, D.-I., Dotson, G., Turner, I., Reiss, L., & Emptage, M. (2003a). Crystal structure of substrate free form of glycerol dehydratase. Journal of Inorganic Biochemistry, 93(1-2), 84–91. https://doi.org/10.1016/s0162-0134(02)00523-8

Liao, D. I., Reiss, L., Turner, I., & Dotson, G. (2003b). Structure of glycerol dehydratase reactivase: a new type of molecular chaperone. Structure (London, England : 1993), 11(1), 109–119. https://doi.org/10.1016/s0969-2126(02)00935-8

Liu, H., Xu, Y., Zheng, Z., & Liu, D. (2010). 1,3-Propanediol and its copolymers: Research, development and industrialization. Biotechnology Journal, 5(11), 1137–1148. https://doi.org/10.1002/biot.201000140

Liu, H.-J., Zhang, D.-J., Xu, Y.-H., Mu, Y., Sun, Y.-Q., & Xiu, Z.-L. (2007). Microbial production of 1,3-propanediol from glycerol by *Klebsiella pneumoniae* under micro-aerobic conditions up to a pilot scale. Biotechnology Letters, 29(8), 1281–1285. https://doi.org/10.1007/s10529-007-9398-2

Luers, F., Seyfried, M., Daniel, R., & Gottschalk, G. (2006). Glycerol conversion to 1,3-propanediol by *Clostridium pasteurianum*: Cloning and expression of the gene encoding 1,3-propanediol dehydrogenase. FEMS Microbiology Letters, 154(2), 337–345. https://doi.org/10.1111/j.1574-6968.1997.tb12665.x

Luo, L. H., Kim, C. H., Heo, S.-Y., Oh, B.-R., Hong, W.-K., Kim, S., Kim, D.-H., & Seo, J.-W. (2012). Production of 3-hydroxypropionic acid through propionaldehyde dehydrogenase pdup mediated biosynthetic pathway in *Klebsiella pneumoniae*. Bioresource Technology, 103(1), 1–6. https://doi.org/10.1016/j.biortech.2011.09.099

Ma, J., Jiang, H., Hector, S. B., Xiao, Z., Li, J., Liu, R., Li, C., Zeng, B., Liu, G.-Q., & Zhu, Y. (2019). Adaptability of *Klebsiella pneumoniae* 2e, a newly isolated 1,3-propanediol-producing strain, to crude glycerol as revealed by genomic profiling. Applied and Environmental Microbiology, 85(10). https://doi.org/10.1128/aem.00254-19

Malaoui, H., & Marczak, R. (2000). Purification and characterization of the 1-3-propanediol dehydrogenase of *Clostridium butyricum* e5. Enzyme and Microbial Technology, 27(6), 399–405. https://doi.org/10.1016/s0141-0229(00)00219-2

Marçal, D., Rêgo, A. T., Carrondo, M. A., & Enguita, F. J. (2009). 1,3-propanediol dehydrogenase from *Klebsiella pneumoniae*: Decameric quaternary structure and possible subunit cooperativity. Journal of Bacteriology, 191(4), 1143–1151. https://doi.org/10.1128/jb.01077-08

Mickelson, M. N., & Werkman, C. H. (1940). The dissimilation of glycerol by coli-aerogenes intermediates. Journal of Bacteriology, 39(6), 709–715. https://doi.org/10.1128/jb.39.6.709-715.1940

Montella, C., Bellsolell, L., Pérez-Luque, R., Badía, J., Baldoma, L., Coll, M., & Aguilar, J. (2005). Crystal structure of an iron-dependent group III dehydrogenase that interconverts l -lactaldehyde and l -1,2-propanediol in *Escherichia coli*. Journal of Bacteriology, 187(14), 4957–4966. https://doi.org/10.1128/jb.187.14.4957-4966.2005

Mori, K., Tobimatsu, T., Hara, T., & Toraya, T. (1997). Characterization, sequencing, and expression of the genes encoding a reactivating factor for glycerol-inactivated adenosylcobalamin-dependent diol dehydratase. Journal of Biological Chemistry, 272(51), 32034–32041. https://doi.org/10.1074/jbc.272.51.32034

Mori, K., & Toraya, T. (1999). Mechanism of reactivation of coenzyme B12-dependent diol dehydratase by a molecular chaperone-like reactivating factor. Biochemistry, 38(40), 13170–13178. https://doi.org/10.1021/bi9911738

Morita, H., Toh, H., Fukuda, S., Horikawa, H., Oshima, K., Suzuki, T., Murakami, M., Hisamatsu, S., Kato, Y., Takizawa, T., Fukuoka, H., Yoshimura, T., Itoh, K., O'Sullivan, D. J., McKay, L. L., Ohno, H., Kikuchi, J., Masaoka, T., & Hattori, M. (2008). Comparative genome analysis of *Lactobacillus reuteri* and *Lactobacillus fermentum* reveal a genomic island for reuterin and Cobalamin Production. DNA Research, 15(3), 151–161. https://doi.org/10.1093/dnares/dsn009

Mu, Y., Teng, H., Zhang, D.-J., Wang, W., & Xiu, Z.-L. (2006). Microbial production of 1,3-propanediol by *Klebsiella pneumoniae* using crude glycerol from biodiesel preparations. Biotechnology Letters, 28(21), 1755–1759. https://doi.org/10.1007/s10529-006-9154-z

Mülhardt, C., & Beese, E. W. (2007). Cloning DNA fragments. Molecular Biology and Genomics, 105–129. https://doi.org/10.1016/b978-012088546-6/50008-7

Nooren, I. M., & Thornton, J. M. (2003). Diversity of protein-protein interactions. The EMBO journal, 22(14), 3486–3492. https://doi.org/10.1093/emboj/cdg359

New England Biolabs. (n.d.). Nebiocalculator® - using the ligation module. NEB. https://international.neb.com/tools-and-resources/video-library/nebiocalculator-using-the-ligation-module

New England Biolabs: Gibson Assembly® Master Mix – Assembly (E2611) (2022). protocols.io https://dx.doi.org/10.17504/protocols.io.cjxupm

OECD. (n.d.). Good laboratory practice (GLP). ©Organisation for Economic Co-operation and Development. https://www.oecd.org/chemicalsafety/testing/good-laboratory-practiceglp.htm

Papanikolaou, S., Fick, M., & Aggelis, G. (2004). The effect of raw glycerol concentration on the production of 1,3-propanediol by *Clostridium butyricum*. Journal of Chemical Technology & Biotechnology, 79(11), 1189–1196. https://doi.org/10.1002/jctb.1103

Pearson, R. G. (1990). Cheminform abstract: Hard and soft acids and bases. the evolution of a chemical concept. ChemInform, 21(34). https://doi.org/10.1002/chin.199034355

Przystałowska, H., Zeyland, J., Kośmider, A., Szalata, M., Słomski, R., & Lipiński, D. (2015a). 1,3-propanediol production by *Escherichia coli* using genes from *Citrobacter freundii* ATCC 8090. Acta Biochimica Polonica, 62(3), 589–597. https://doi.org/10.18388/abp.2015_1061

Przystałowska, H., Zeyland, J., Szymanowska-Powałowska, D., Szalata, M., Słomski, R., & Lipiński, D. (2015b). 1,3-propanediol production by new recombinant *Escherichia coli* containing genes from pathogenic bacteria. Microbiological Research, 171, 1–7. https://doi.org/10.1016/j.micres.2014.12.007

Ragauskas, A. J., Williams, C. K., Davison, B. H., Britovsek, G., Cairney, J., Eckert, C. A., Frederick, W. J., Hallett, J. P., Leak, D. J., Liotta, C. L., Mielenz, J. R., Murphy, R., Templer, R., &

Tschaplinski, T. (2006). The path forward for biofuels and biomaterials. Science, 311(5760), 484–489. https://doi.org/10.1126/science.1114736

Ratelade, J., Miot, M.-C., Johnson, E., Betton, J.-M., Mazodier, P., & Benaroudj, N. (2009). Production of recombinant proteins in the lon-deficient BL21(DE3) strain of *Escherichia coli* in the absence of the Dnak Chaperone. Applied and Environmental Microbiology, 75(11), 3803–3807. https://doi.org/10.1128/aem.00255-09

REN21, P. S. (2017). Renewables 2017 global status report. Secretariat Renewable Energy Policy Network for the, 21.

Rezaei, R. (2013). Bio-based C-3 Platform Chemical: Biotechnological Production and -Conversion of 3- Hydroxypropionaldehyde. [Doctoral Thesis (compilation), Biotechnology]. Lund University.

Rouhany, M., & Montgomery, H. (2018). Global biodiesel production: The state of the art and impact on climate change. Biofuel and Biorefinery Technologies, 1–14. https://doi.org/10.1007/978-3-030-00985-4_1

Ruch, F. E., & Lin, E. C. (1975). Independent constitutive expression of the aerobic and anaerobic pathways of glycerol catabolism in *Klebsiella aerogenes*. Journal of Bacteriology, 124(1), 348–352. https://doi.org/10.1128/jb.124.1.348-352.1975

Ruzheinikov, S. N., Burke, J., Sedelnikova, S., Baker, P. J., Taylor, R., Bullough, P. A., Muir, N. M., Gore, M. G., & Rice, D. W. (2001). Glycerol dehydrogenase. Structure, 9(9), 789–802. https://doi.org/10.1016/s0969-2126(01)00645-1

Sankaranarayanan, M., Seol, E., Kim, Y., Chauhan, A. S., & Park, S. (2017). Measurement of crude-cell-extract glycerol dehydratase activity in recombinant *Escherichia coli* using coupled-enzyme reactions. Journal of Industrial Microbiology and Biotechnology, 44(3), 477–488. https://doi.org/10.1007/s10295-017-1902-7

Saxena, R. K., Anand, P., Saran, S., & Isar, J. (2009). Microbial production of 1,3-propanediol: Recent developments and emerging opportunities. Biotechnology Advances, 27(6), 895–913. https://doi.org/10.1016/j.biotechadv.2009.07.003

Seifert, C., Bowien, S., Gottschalk, G., & Daniel, R. (2001). Identification and expression of the genes and purification and characterization of the gene products involved in reactivation of coenzyme B12-dependent glycerol dehydratase of *Citrobacter freundii*. European Journal of Biochemistry, 268(8), 2369–2378. https://doi.org/10.1046/j.1432-1327.2001.02123.x

Singh, K., Ainala, S. K., & Park, S. (2021). Metabolic Engineering of *Lactobacillus reuteri* DSM 20,016 for improved 1,3-propanediol production from glycerol. Bioresource Technology, 338, 125590. https://doi.org/10.1016/j.biortech.2021.125590

Slininger, P. J., Bothast, R. J., & Smiley, K. L. (1983). Production of 3-hydroxypropionaldehyde from glycerol. Applied and Environmental Microbiology, 46(1), 62–67. https://doi.org/10.1128/aem.46.1.62-67.1983

Strandberg, L., & Enfors, S. O. (1991). Factors influencing inclusion body formation in the production of a fused protein in *Escherichia coli*. Applied and Environmental Microbiology, 57(6), 1669–1674. https://doi.org/10.1128/aem.57.6.1669-1674.1991

Sun, J., van den Heuvel, J., Soucaille, P., Qu, Y., & Zeng, A.-P. (2003). Comparative genomic analysis of DHA regulon and related genes for anaerobic glycerol metabolism in bacteria. Biotechnology Progress, 19(2), 263–272. https://doi.org/10.1021/bp025739m

Sun, Y.-Q., Shen, J.-T., Yan, L., Zhou, J.-J., Jiang, L.-L., Chen, Y., Yuan, J.-L., Feng, E. M., & Xiu, Z.-L. (2018). Advances in bioconversion of glycerol to 1,3-propanediol: Prospects and challenges. Process Biochemistry, 71, 134–146. https://doi.org/10.1016/j.procbio.2018.05.009

Tong, I. T., Liao, H. H., & Cameron, D. C. (1991). 1,3-propanediol production by *Escherichia coli* expressing genes from the *Klebsiella pneumoniae* DHA regulon. Applied and Environmental Microbiology, 57(12), 3541–3546. https://doi.org/10.1128/aem.57.12.3541-3546.1991

Toraya, T. (2000). Radical catalysis of B 12 enzymes: Structure, mechanism, inactivation, and reactivation of Diol and glycerol dehydratases. Cellular and Molecular Life Sciences (CMLS), 57(1), 106–127. https://doi.org/10.1007/s000180050502

Toraya, T., Shirakashi, T., Kosuga, T., & Fukui, S. (1976). Substrate specificity of coenzyme B12-dependent diol dehydrase: Glycerol as both a good substrate and a potent inactivator. Biochemical and Biophysical Research Communications, 69(2), 475–480. https://doi.org/10.1016/0006-291x(76)90546-5

Toraya, T., Ushio, K., Fukui, S., & Hogenkamp, P. C. (1977). Studies on the mechanism of the adenosylcobalamin-dependent diol dehydrase reaction by the use of analogs of the coenzyme. Journal of Biological Chemistry, 252(3), 963–970. https://doi.org/10.1016/s0021-9258(19)75192-8

Umare, S. S., Chandure, A. S., & Pandey, R. A. (2007). Synthesis, characterization and biodegradable studies of 1,3-propanediol based polyesters. Polymer Degradation and Stability, 92(3), 464–479. https://doi.org/10.1016/j.polymdegradstab.2006.10.007

Wang, F., Qu, H., Zhang, D., Tian, P., & Tan, T. (2007). Production of 1,3-propanediol from glycerol by recombinant *E. coli* using incompatible plasmids system. Molecular Biotechnology, 37(2), 112–119. https://doi.org/10.1007/s12033-007-0041-1

Widayat, Wibowo, A. D., & Hadiyanto. (2013). Study on production process of biodiesel from rubber seed (Hevea brasiliensis) by in situ (trans)esterification method with acid catalyst. Energy Procedia, 32, 64–73. https://doi.org/10.1016/j.egypro.2013.05.009

Willke, T., & Vorlop, K.-D. (2004). Industrial bioconversion of renewable resources as an alternative to conventional chemistry. Applied Microbiology and Biotechnology, 66(2), 131–142. https://doi.org/10.1007/s00253-004-1733-0

Witt, U., Müller, R.-J., Augusta, J., Widdecke, H., & Deckwer, W.-D. (1994). Synthesis, properties and biodegradability of polyesters based on 1,3-propanediol. Macromolecular Chemistry and Physics, 195(2), 793–802. https://doi.org/10.1002/macp.1994.021950235

Yamanishi, M., Yunoki, M., Tobimatsu, T., Sato, H., Matsui, J., Dokiya, A., Iuchi, Y., Oe, K., Suto, K., Shibata, N., Morimoto, Y., Yasuoka, N., & Toraya, T. (2002). The crystal structure of coenzyme B12-dependent glycerol dehydratase in complex with cobalamin and propane-1,2-diol. European Journal of Biochemistry, 269(18), 4484–4494. https://doi.org/10.1046/j.1432-1033.2002.03151.x

Yang, Q., Tomlinson, A. J., & Naylor, S. (1998). Sample preparation. Journal of Chromatography Library, 95–140. https://doi.org/10.1016/s0301-4770(08)60301-2

Yazdani, S. S., & Gonzalez, R. (2007). Anaerobic fermentation of glycerol: A path to economic viability for the biofuels industry. Current Opinion in Biotechnology, 18(3), 213–219. https://doi.org/10.1016/j.copbio.2007.05.002

Yu, C., Cao, Y., Zou, H., & Xian, M. (2010). Metabolic engineering of *Escherichia coli* for biotechnological production of high-value organic acids and alcohols. Applied Microbiology and Biotechnology, 89(3), 573–583. https://doi.org/10.1007/s00253-010-2970-z

Zeng, A.-P., & Biebl, H. (2002). Bulk chemicals from biotechnology: The case of 1,3-propanediol production and the new trends. Tools and Applications of Biochemical Engineering Science, 239–259. https://doi.org/10.1007/3-540-45736-4_11

Zheng, D., & Lu, T. (1996). Electrochemical reactions of cyanocobalamin in acidic media. Journal of Electroanalytical Chemistry, 429(1–2), 61–65. https://doi.org/10.1016/s0022-0728(96)05021-8

© 2023 SnapGene. (2023a). pCDFDuet-1 sequence and map. SnapGene by Dotmatics. Retrieved April 28, 2023, from https://www.snapgene.com/plasmids/pet_and_duet_vectors_(novagen)/pCDFDuet-1

© 2023 SnapGene. (2023b). Pet-28A(+) sequence and map. SnapGene by Dotmatics. Retrieved April 28, 2023, from https://www.snapgene.com/plasmids/pet_and_duet_vectors_(novagen)/pET-28a(%2B)

Appendix

Figures

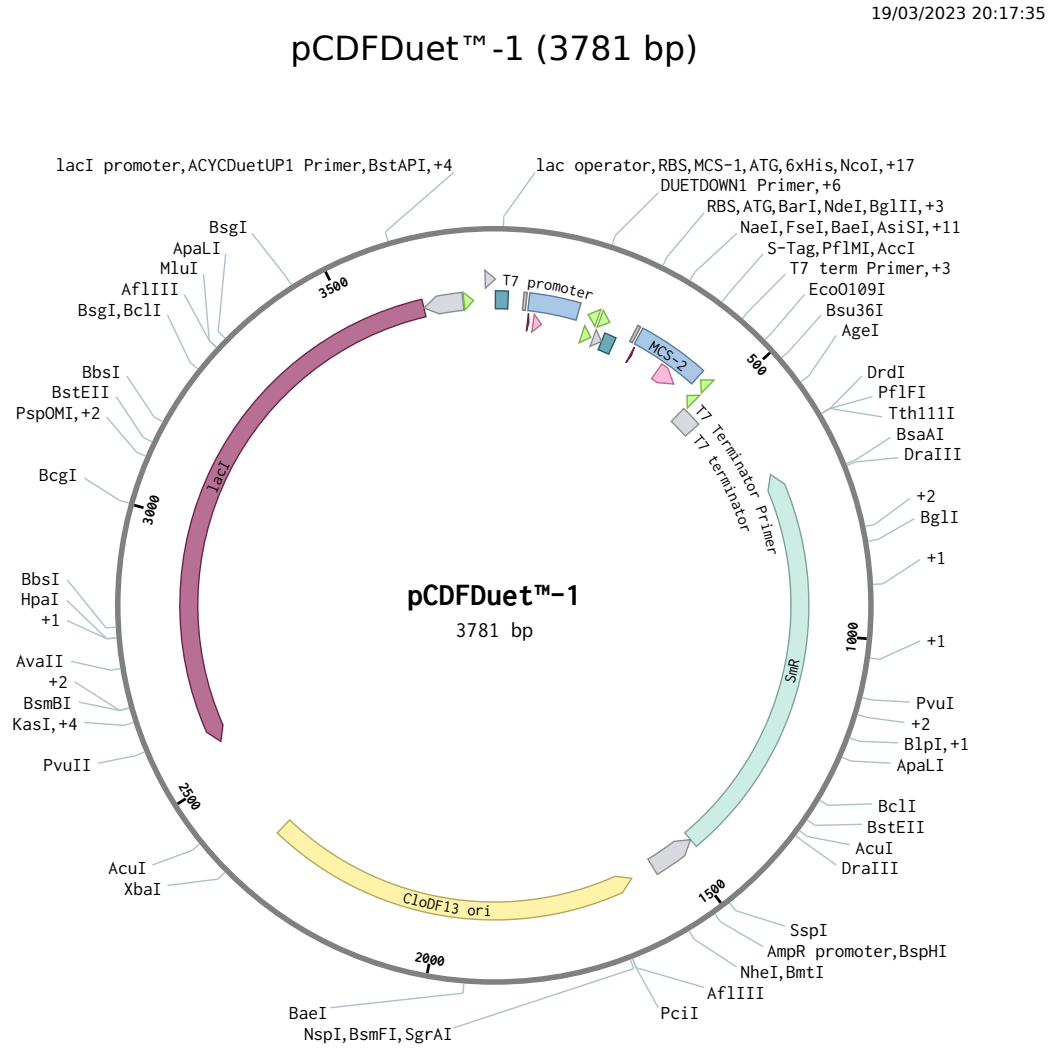

Figure A1: Bacterial vector enabling the simultaneous expression of two genes. It has a CloDF13 (CDF) origin of replication (© 2023 SnapGene, 2023a).

pET28a(+) (5369 bp)

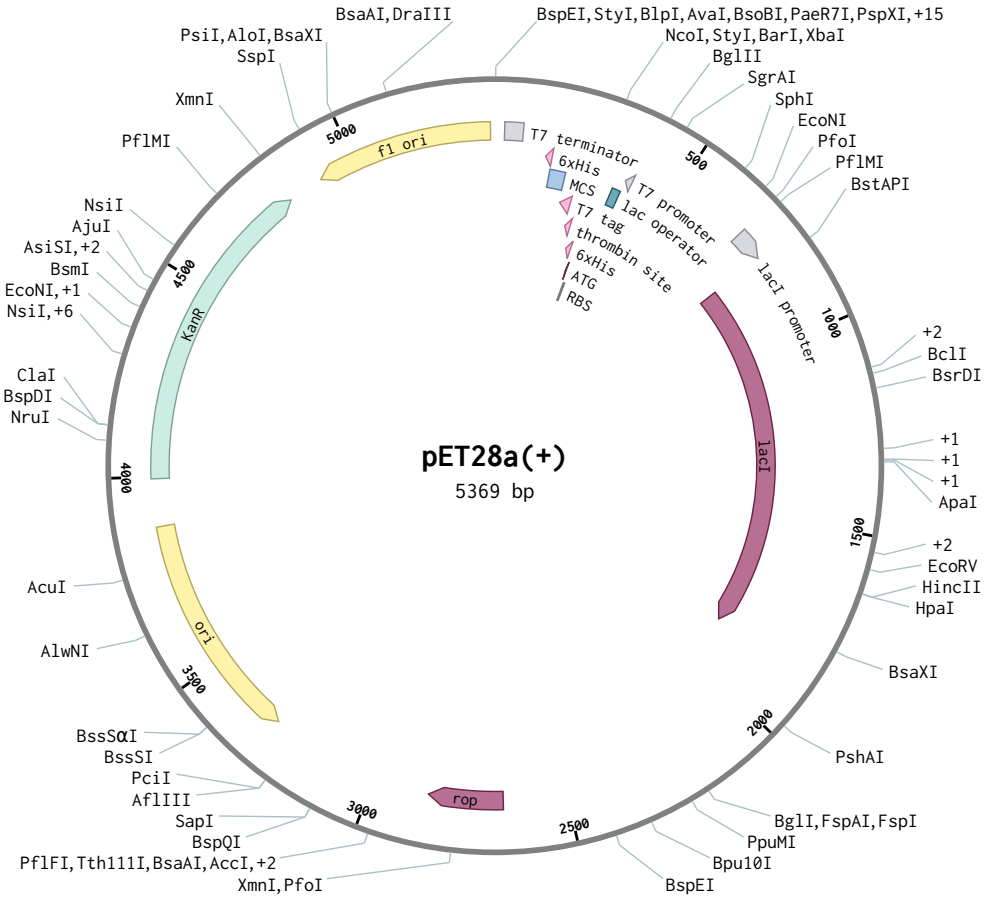

Figure A2: Bacterial vector for the expression of thrombin-sited, 6xHis-tagged proteins (© 2023 SnapGene, 2023b).

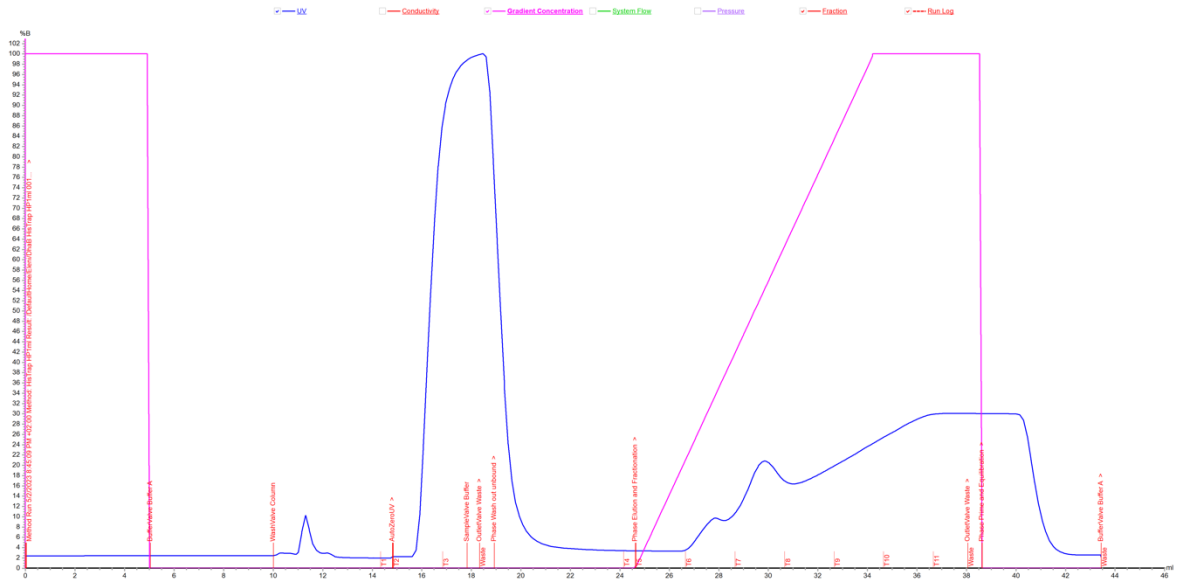

Figure A3: Immobilized metal affinity chromatography (IMAC) purification chromatogram of GDHt protein. The x-axis represents the elution buffer volume (mL), while the y-axis the gradient concentration of the elution buffer (%). The His_6-tagged protein elutes in the range between 10% to 55% gradient concentration (fraction T7).

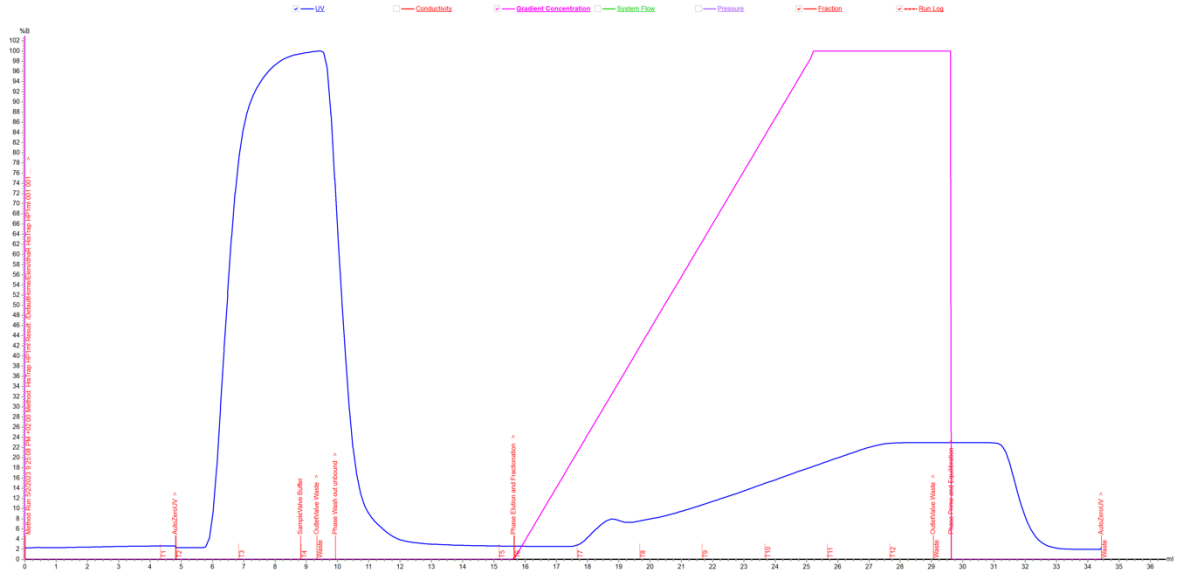

Figure A4: Immobilized metal affinity chromatography (IMAC) purification chromatogram of GDHtR protein. The x-axis represents the elution buffer volume (mL), while the y-axis the gradient concentration of the elution buffer (%). The His_6-tagged protein elutes in the range between 7% to 57% gradient concentration (fractions T8).

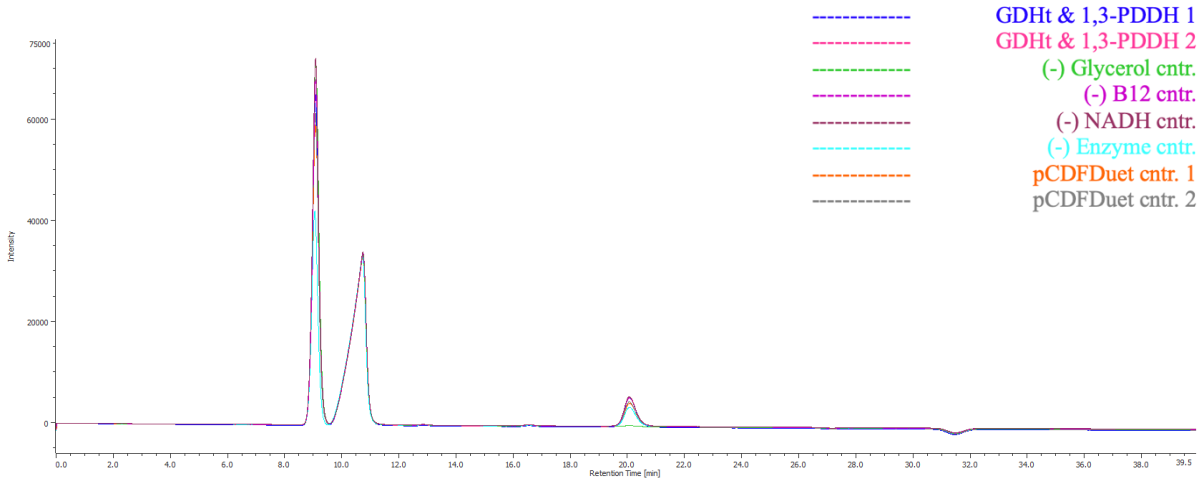

Figure A5: High performance liquid chromatography (HPLC) chromatogram of coupled-enzyme-reaction activity assay. The crude cell lysate soluble (S) fraction of E. coli BL21 (DE3) cells, coexpressing GDHt and 1,3-PDDH were used for the assay. The reaction was carried out in 35 mM potassium phosphate buffer (pH 8.0, filter sterilized), 10 mM glycerol, 0.015 mM coenzyme B12 and 0.15 mM NADH. The x-axis represents the retention time in minutes and the y-axis the signal intensity.

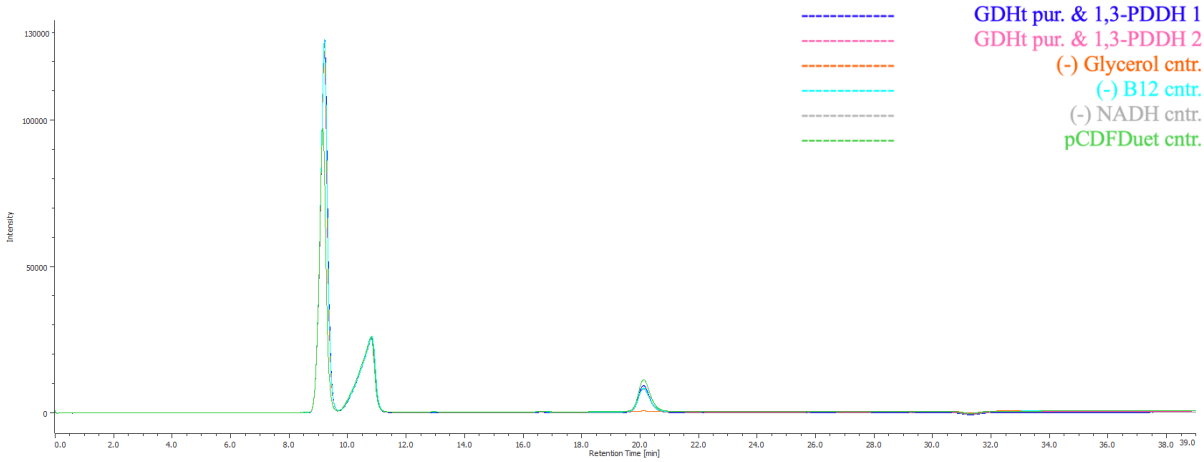

Figure A6: High performance liquid chromatography (HPLC) chromatogram of coupled-enzyme-reaction activity assay. The purified GDHt enzyme together with the crude cell lysate soluble (S) fraction of E. coli BL21 (DE3) cells, expressing 3-PDDH were used for the assay. The reaction was carried out in 35 mM potassium phosphate buffer (pH 8.0, filter sterilized), 10 mM glycerol, 0.015 mM coenzyme B12 and 0.15 mM NADH. The x-axis represents the retention time in minutes and the y-axis the signal intensity.

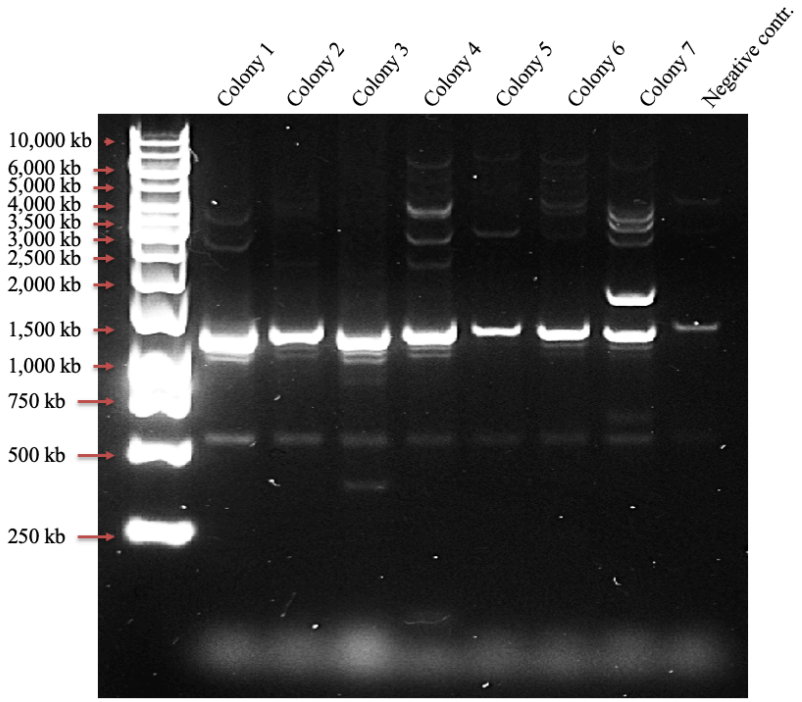

Figure A7: Agarose gel electrophoresis of colony PCR products following transformation of DH5a competent cells with the ligated pCDFDuet™-1_orfX/orfZ construct. The GeneRuler 1 kb DNA ladder (0.5 µg × mL^{-1}) (Thermo Scientific) was used as a size reference. Lanes 2-8 correspond to the eight colony samples that were analyzed, while lane 9 represents the negative control containing MilliQ water instead of a DNA template.

Tables

Table A1: Primers that were used in this work. The primers' sequence, length, Tm (℃), GC content (%) and source is indicated.

Primer[5]	Sequence (orientation 5' to 3')[6]	Length	Tm (°C)	GC (%)	Source
Duet fwd.	**ACG CAA TTA G**CA AGC TTG CGG CCG CAT AAT G	31	66,1	51,6	IDT, USA
Duet rev.	**TCA ATG GCA** TCG GAT CCT GGC TGT GGT G	28	65,8	57,1	IDT, USA
Duet_dhaR fwd.	**CCA GGA TC**C GAT GCC ATT GAT TGC TGG AAT AG	32	63.4	50	IDT, USA
Duet_dhaR rev.	**CGC AAG CT**T GCT AAT TGC GTT CGC TCA G	28	63.9	53.6	IDT, USA
T7 fwd.	TAA TAC GAC TCA CTA TAG GG	20	53,2	40	Eurofins, LU
T7 rev.	CTA GTT ATT GCT CAG CGG T	19	54,5	47	Eurofins, LU

Table A2: Enzymes and kits that were used in this work.

Name	Source & Reference
DMSO, 100%	Thermo Scientific, USA, LOT: 01187703
dNTP mix, 10mM each	Thermo Scientific, USA, LOT: 00166700
DNA Gel Loading Dye, 6X	Thermo Scientific, USA, LOT: 00379937
DreamTaq Green PCR Master Mix, 2X	Thermo Scientific, USA, LOT: 00861999
FastDigest Buffer, 10X	Thermo Scientific, USA, LOT: 00175029
FastDigest BamHI	Thermo Scientific, USA, LOT: 00095716
FastDigest HindIII	Thermo Scientific, USA, LOT: 00102405
GelGreen Nucleic Acid Stain, 10,000X	Biotium, USA, LOT: 20G0121
GeneJET PCR Purification Kit	Thermo Scientific, USA, LOT: 01093944
GeneJET Plasmid Miniprep Kit	Thermo Scientific, USA, LOT: 01238801
GeneRuler 1 kb DNA ladder (0.5 µg × mL^{-1})	Thermo Scientific, USA, LOT: 00107355
Laemmli Sample Buffer, 4x	BIO-RAD, USA
Mini-PROTEAN® TGX Stain-Free™ Protein Gels, 15 well, 15 µl, 4-20%	BIO-RAD, USA, Batch: 64518278
NEBuilder® HiFi DNA Assembly Master Mix	New England Biolabs, USA, LOT: 10156827
NEBuilder® Positive Control	New England Biolabs, USA, LOT: 10157948
Orange DNA Loading Dye, 6X	Thermo Scientific, USA, LOT: 00269046
Phusion™ High-Fidelity DNA Polymerase (2 U/µL)	Thermo Scientific, USA, LOT: 01079020
Phusion™ GC buffer (contains 7.5 mM $MgCl_2$), 5X	Thermo Scientific, USA, LOT: 01178531
Phusion™ High-Fidelity buffer (contains 7.5 mM $MgCl_2$), 5X	Thermo Scientific, USA, LOT: 01205238
Precision Plus Protein™, Unstained Protein Standards	BIO-RAD, USA, Batch: 64466346
QIAquick® Gel Extraction Kit (50)	QIAGEN, Germany, LOT: 172029437
T4 DNA ligase, 500 Weiss U/µL	Thermo Scientific, USA, LOT: 01102990
T4 DNA ligase buffer, 10X	Thermo Scientific, USA, LOT: 00123962

[5] Fwd, forward primer; Rev, reverse primer.
[6] Bold base pairs in primer sequences indicate overhangs.

Table A3: Buffers and Growth media that were used in this work. For each buffer, the components CAS number, concentration, and source is indicated.

Buffer & Use	**Components**	**CAS no.**	**Conc.**	**Source & Reference**
Binding Buffer (pH 8, 35 mM) for protein purification	Imidazole 99%	288-32-4	20 mM	Sigma Aldrich, USA, LOT: WXBD3484V
	Potassium Phosphate Dibasic (K_2HPO_4) 98+%	7758-11-4	32.72 mM	Thermo Scientific, USA, LOT: 10220399
	Potassium Phosphate Monobasic (KH_2PO_4) 98+%	7778-77-0	2.283 mM	Thermo Scientific, USA, LOT: 10231328
	Sodium Chloride (NaCl) 99.0% min	7647-14-5	500 mM	Thermo Scientific, USA, LOT: Z15H053
Citrate Buffer (pH 3.6, 100 mM) for MBTH method	Citric Acid ($C_6H_8O_7$)	77-92-9	75.99 mM	Merck, Germany, LOT: 8.18707.1000
	Sodium Citrate Dihydrate ($Na_3C_6H_5O_7 \cdot 2H_2O$)	6132-04-3	24.01 mM	Merck, Germany, LOT: 1.06448.1000
Elution Buffer (pH 8, 35 mM) for protein purification	Imidazole 99%	288-32-4	500 mM	Sigma Aldrich, USA, LOT: WXBD3484V
	Potassium Phosphate Dibasic (K_2HPO_4) 98+%	7758-11-4	32.72 mM	Thermo Scientific, USA, LOT: 10220399
	Potassium Phosphate Monobasic ($K_3H_2PO_4$) 98+%	7778-77-0	2.283 mM	Thermo Scientific, USA, LOT: 10231328
	Sodium Chloride (NaCl) 99.0% min	7647-14-5	500 mM	Thermo Scientific, USA, LOT: Z15H053
LB Agar for agar plate preparation	Agar Powder	9002-18-0	15 g/L	VWR Chemicals, USA, LOT: 21J074122
	Sodium Chloride (NaCl, crystalline) 99.0%	7647-14-5	10 g/L	Thermo Scientific, USA, LOT: Z15H053
	Tryptone	91079-40-2	10 g/L	Thermo Scientific, USA, LOT: 1280084
	Yeast Extract powder	8013-01-2	5 g/L	Sigma Aldrich, USA, LOT: BCCG1352
LB Broth for liquid cell culture	Sodium Chloride (NaCl, crystalline) 99.0% min	7647-14-5	10 g/L	Thermo Scientific, USA, LOT: Z15H053
	Bacto™ Tryptone	91079-40-2	10 g/L	Thermo Scientific, USA, LOT: 1280084
	Yeast Extract powder	8013-01-2	5 g/L	Sigma Aldrich, USA, LOT: BCCG1352
LB Broth from LB powder	Luria Broth (Miller's LB Broth Base)v	-	25 g/L	Thermo Scientific, USA, LOT: 203241
Potassium Phosphate Buffer (pH 8, 35 mM)	Potassium Phosphate Dibasic (K_2HPO_4) 98+%	7758-11-4	32.72 mM	Thermo Scientific, USA, LOT: 10220399
	Potassium Phosphate Monobasic (KH_2PO_4) 98+%	7778-77-0	2.283 mM	Thermo Scientific, USA, LOT: 10231328
Resuspension buffer (pH 8, 50 mM)	Potassium Chloride (KCl)	7447-40-7	50 mM	Merck, Germany, LOT: 1.04936.1000
	Potassium Phospate Buffer (pH 8, 35 mM)	-	50 mM	-
Sulfuric acid (0.5 mM) mobile phase for HPLC	Sulfuric acid (H_2SO_4), 95.0-98.0%	7664-93-9	0.5 mM	Sigma-Aldrich, USA, LOT: MKCR6032
	Acetic acid (CH_3COOH) (glacial), 100%	87-51-4	1000 mM	Merck, Germany, LOT: 1.00063.2511

Buffer & Use	Components	CAS no.	Conc.	Source & Reference
Tris acetate EDTA (TAE) buffer for gel preparation (50X)	Tris base (tris-(hydroxymethyl)-aminomethane) ($C_4H_{11}NO_3$)	77-86-1	2000 mM	ITW Reagents, Italy, LOT: 9U011903
	EDTA disodium salt dihydrate ($C_{10}H_{14}N_2Na_2O_8 \cdot 2H_2O$)	6381-92-6	50 mM	AppliChem GmbH, Germany, LOT: 9D010690
TfbI (transformation buffer I) (pH 5.8)	Calcium Chloride Dihydrate ($CaCl_2 \cdot 2H_2O$)	10035-04-8	10 mM	Merck, Germany, LOT: 1.02382.1000
	Glycerol bidistilled 99.5%	56-81-5	15% v/v	VWR Chemicals, USA, LOT: 24388.320
	Manganese(II) chloride tetrahydrate ($MnCl_2 \cdot 4H_2O$) >99%	13446-34-9	50 mM	Sigma Aldrich, USA, LOT: SLBX9249
	Potassium acetate (CH_3COOK)	127-08-2	30 mM	Merck, Germany, LOT: 1.04820.1000
	Rubidium chloride (RbCl), 99.8+%	7791-11-9	100 mM	Thermo Scientific, USA, LOT: A0397570
TfbII (transformation buffer II) (pH 6.5)	Calcium Chloride Dihydrate ($CaCl_2 \cdot 2H_2O$)	10035-04-8	75 mM	Merck, Germany, LOT: 1.02382.1000
	Glycerol bidistilled 99.5%	56-81-5	15% v/v	VWR Chemicals, USA, LOT: 24388.320
	MOPS sodium salt >99.5%	71119-22-7	10 mM	Sigma Aldrich, USA, LOT: SLBM8528V
	Rubidium chloride (RbCl), 99.8+%	7791-11-9	10 mM	Thermo Scientific, USA, LOT: A0397570

Table A4: Other chemicals that were used in this work. For each chemical compound, the CAS number, and source is indicated.

Substance	CAS no.	Source & Reference
1,2-Propandiol 99.5+%, A.C.S. Reagent	57-55-6	Sigma-Aldrich, USA, LOT: 05203EE-207
2-Mercaptoethanol (C_2H_6OS), 99%	60-24-2	Sigma-Aldrich, USA, LOT: BCCB9882
3-Methyl-2-benzothiazolinone-hydrazone hydrochlorideB (MBTH) ($C_8H_9N_3S \cdot HCl \cdot H_2O$)	4338-98-1	Sigma-Aldrich, USA, LOT: BCCJ0238
Agarose standard	9012-36-6	Saveen Werner AB, Sweden, LOT: 008149.01
beta-Nicotinamide adenine dinucleotide disodium salt (NADH), 95+%, reduced	1949720-50-6	Acros Organics, Germany, LOT: A0420477
Certified™ Molecular Biology Agarose	9012-36-6	BIO-RAD, USA, LOT: 1613102
D(+)-Glycose Anhydrous ($C_6H_{12}O_6$)	50-99-7	VWR Chemicals, USA, LOT: 10H090027
Ethanol (EtOH), 99.5 %	64-17-5	SOLVECO, Sweden, LOT: 6095182
Hydrochloric acid (HCl), 36.5-38.0%	7647-01-0	Sigma-Aldrich, USA, LOT: MKCM5691
Isopropyl-beta-D-thiogalactopyranoside (IPTG), dioxane-free	367-93-1	Thermo Scientific, USA, LOT: 00060202
Magnesium Chloride ($MgCl_2$), 50 mM	7786-30-3	Thermo Scientific, USA, LOT: 00840879
Potassium Chloride (KCl)	7447-40-7	Merck, Germany, LOT: 1.04936.1000
Sodium hydroxide (NaOH) (low chloride), ACS, 97.0%	1310-73-2	Alfa Aesar, Germany, LOT: T11D014
Sulfuric acid (H_2SO_4), 95.0-98.0%	7664-93-9	Sigma-Aldrich, USA, LOT: MKCR6032
Vitamin B_{12}, ≥98%	68-19-9	Sigma-Aldrich, USA, LOT: MKCS3192

Table A5: Equipment and software used in this work.

Device	Model	Manufacturer
Analytical Balance	ADVENTURER™ Pro Precision Electronic Balance AV2102C, SN: 8729080044 (for gel preparation)	OHAUS Corporation, Switzerland
	Balance EL3002 3,200g portable top pan x 10mg, SN: 1231220727 (for centrifuge balancing)	Mettler-Toledo, China
	Sartorius BCE1241-1S Entris® II Series Analytical Balance, 120 g x 0.1 mg, SN: 0043001945	Sartorius Lab Instruments GmbH & Co. KG, Germany
	Sartorius BCE2201I-1S Entris® II Basic Essential Toploading Balance with Internal Calibration, 2200 g x 100 mg; 100 to 240 VAC, 50/60 Hz, SN: 0043204202	Sartorius Lab Instruments GmbH & Co. KG, Germany
Autoclave	Vertical Floor-Standing Autoclave Systec VE-150, SN: 8658	Systec GmbH & Co. KG, Germany
Benchling software	Benchling R&D cloud, online software	Benchling, USA
Freezer	DF350-86 Ultra Low Temperature Freezer (-80°C), SN: DF310195	Snijders scientific, Netherlands
Fume cupboard	Fume cupboard with FLOCHECK V monitor	Lindinvent AB, Sweden
Centrifuge	Himac CT15E, SN: 880351	Hitachi Koki Co., Taiwan
	MiniStar silverline, Microcentrifuge, SN: 10051144	VWR International, Korea
	Refrigerated benchtop centrifuge Sigma 3-16KL, SN: 142965	SIGMA Laborzentrifugen GmbH, Germany
	Sorvall™ Legend™ Micro 17 Microcentrifuge 75002430, SN:42124310	Thermo Scientific, USA
	Sorvall LYNX 4000 Superspeed Centrifuge 75006580, SN: 41718653	Thermo Scientific, USA
Chromatography software	UNICORN™ 7 control software for chromatography, filtration, oligo synthesis and bioreactors	Cytiva, United Kingdom
Chromatography system	ÄKTA™ start protein purification system AC/DC input 100 - 240 V AC, SN: 2179531	GE Healthcare Bio-Sciences AB, Sweden
Chromatography column	HisTrap™ High Performance His tag protein purification column	Cytiva, United Kingdom
Electrophoresis System	Mini Protean® Tetra Cell, SN: 552BR 208189	BIO-RAD, USA
	PowerPac™ Basic Power Supply, SN: 041BR310914	BIO-RAD, USA
	Wide Mini-Sub® Cell GT, SN: 258BR038461	BIO-RAD, USA
Expasy software	Expasy 3.0, the Swiss Bioinformatics Resource Portal	Swiss Institute of Bioinformatics, Switzerland
Gel Illuminator	Gel-Bright™ LED Gel Illuminator	Biotium Inc., China
Gel Imaging System	GelDoc Go Imaging System, SN: 730BR10991	BIO-RAD, USA
Heating Block	3001 series magnetic stirring hotplate, SN: 504.10100.00	Heidolph Instruments, Germany
	BTD Dry Block Heater for Microtubes, SN: 010412-1012-0176	Grant Instruments Ltd, United Kingdom
HPLC	AS-4150/4250 RHPLC system with RI-4030 refractive index detector, CO-4061 column oven, PU-4180 pump, SN: A022261687	Jasco Corporation, Japan
HPLC column	Aminex® HPX-87H Ion exclusion HPLC organic acid analysis column 300 mm x 7.8 mm, SN: 443409	BIO-RAD, USA
HPLC software	ChromNav Version 2.03.03 HPLC software	Jasco Corporation, Japan
Ice maker	Ice Queen IG50C AIRE 220/50 R290, SN: 18566659	TV Ice Makers Inc., Spain
Incubator	T 1056 U Incubator	Termaks AS, Norway
Laminar Flow Hood	Cellgard ES Energy Saver Class II, Type A2 Laminar Flow Biological Safety Cabinet Model NU-400E, SN: 142693021611	NuAire Inc., USA
	Type S-2010 1.2 Sterile Cabinet, SN: 22163C	Heto-Holten, Denmark

Device	Model	Manufacturer
Milli-Q® Water System	Milli-Q® IQ 7000 Ultrapure Lab Water System, SN: F9JA42046	Merck KGaA, France
Magnetic stirrer	Hei-Mix S Magnetic Stirrer, SN: 111050806	Heidolph Instruments, Germany
NEBioCalculator®	Version 1.15.3, online software	New England Biolabs, USA
pH meter	Thermo Electron Orion PerpHecT Model 310 pH Meters, SN: 002856	Orion Research Inc., USA
Pipettes	Sartorius Tacta™ Mechanical Pipettes 10, 100, 1000	Thermo Fisher Scientific Inc., USA
Shaking Incubator	Ecotron Table-top Incubator Shaker, SN: S-000126380 and S-000126388	INFORS HT (Infors AG), Switzerland
SnapGene software	SnapGene 6.2	Dotmatics, USA
Sonicator	Ultrasonic processor UP400S (400 watts, 24kHz)	Hielscher Ultrasonics GmbH, Germany
Spectrophotometer	BioSpec-nano spectrophotometer for Life Science 206-26300-58, SN: A11645800976	Shimadzu Corporation, Japan
	Evolution™ 300 UV-Vis Spectrophotometer, SN:EVOP228001 with Peltier Temperature Control, SN: EVOP300003 VISIONpro™ Software	Thermo Scientific, USA
	Lambda Bio+ spectrophotometer L7110186, SN: B0186L-3254	Perkin Elmer Ltd, United Kingdom
Thermocycler	CFX96™ Touch Real-Time PCR Detection System, SN: 785BR20057	BIO-RAD, Singapore
	Labcycler Basic (011-103), SN: 1119320156	SensoQuest GmbH, Germany
	T100™ PCR Thermal Cycler, SN: 621BR53540	BIO-RAD, Singapore
Vortex Mixer	Reax Top Vortex Mixer 541.10000.00 0, SN: 019800617	Heidolph Instruments, Germany
	Vortex Mixer Type VM20	Chiltern Scientific Enterprise, United Kingdom
Washing machine	PG 8593 (208V) Laboratory glassware washer with liquid dispensing & DryPlus drying GG05, SN: 018449200	Miele & Cie. KG., Germany
Water bath	ECO Silver Circulation Thermostat with ECO E10S Stainless Steel Bath, SN: S170000034	LAUDA DR. R. WOBSER GMBH & CO. KG, Germany

Raw data and calculations

MBTH method for GDHt activity determination

The MBTH technique was employed to evaluate the activity of GDHt enzyme and investigate the effect of the GDHtR reactivase on this activity. Crude cell lysate containing the two enzymes, was used for the analysis. One unit (U) of enzyme activity was determined as the quantity of GDHt enzyme needed to convert 1 mol of 1,2-propanediol into propionaldehyde per minute. The activity calculations were based on absorbance measurements at 305 nm, using the Beer-Lambert's law ($A = \varepsilon \times c \times l$), where ε represents the apparent molar extinction coefficient of the colorful product generated from 3-HPA ($\varepsilon = 13.3 \times 103\ M^{-1} \times cm^{-1}$) and l represents the path length of the cuvette (l = 1 cm). The calculations, including the raw data, are presented in **Table A6**. The final reaction volume (V = 2.5 mL) and the volume of the added enzyme (V = 0.1 mL) were also taken into account in the calculations.

Table A6: Raw data and enzymatic activity calculations. The 3-methyl-2-benzothialzolinone hydrazone (MBTH) analysis was performed with crude cell lysate GDHt (dhaB) and GDHtR (orfX/orfZ) protein expression samples (soluble [S] and insoluble [I] fraction). The absorbance values at 305 nm were used to calculate 1 Unit of enzymatic activity (U = µmol × min^{-1}), according to Beer-Lambers' law.

Sample	OD_{305}	ΔA (min^{-1})	C (mol × L^{-1} × min^{-1})	C (µmol × min^{-1}) per 0,1 mL enzyme	Units x mL^{-1}
GDHt [I]	1,805	0,1805	1,36E-05	3,39E-03	3,39E+01
GDHt + GDHtR [I]	3,32	0,332	2,50E-05	6,24E-03	6,24E+01
GDHt [S]	0,571	0,0571	4,29E-06	1,07E-03	1,07E+01
GDHt + GDHtR [S]	1,048	0,1048	7,88E-06	1,97E-03	1,97E+01
(-) Enzyme	-0,034	-0,0034	-2,56E-07	-6,39E-05	-6,39E-01
(-) 1,2-Propanediol [S]	0,577	0,0577	4,34E-06	1,08E-03	1,08E+01
(-) B12 [S]	0,568	0,0568	4,27E-06	1,07E-03	1,07E+01
pCDFDuet [I]	-0,015	-0,0015	-1,13E-07	-2,82E-05	-3,13E-01
pCDFDuet [S]	-0,015	-0,0015	-1,13E-07	-2,82E-05	-3,13E-01

Similarly, the calculations for the MBTH assay of the purified enzymes, including the raw data, are presented in **Table A7**. The final reaction volume (V = 5.0 mL) and the volume of the added enzyme (V = 0.1 mL) were also taken into account in the calculations.

Table A7: Raw data and enzymatic activity calculations. The 3-methyl-2-benzothialzolinone hydrazone (MBTH) analysis was performed with purified GDHt and GDHtR enzymes. The absorbance values at 305 nm were used to calculate 1 Unit of enzymatic activity (U = µmol × min^{-1}), according to Beer-Lambers' law.

Sample	OD_{305}	ΔA (min^{-1})	C (mol × L^{-1} × min^{-1})	C (µmol × min^{-1}) per 0,1 mL enzyme	Units x mL^{-1}
GDHt 1 [S]	1,805	0,1805	1,36E-05	3,39E-03	3,39E+01
GDHt 2 [S]	3,32	0,332	2,50E-05	6,24E-03	6,24E+01
GDHt + GDHtR 1 [S]	0,571	0,0571	4,29E-06	1,07E-03	1,07E+01
GDHt + GDHtR 2 [S]	1,048	0,1048	7,88E-06	1,97E-03	1,97E+01
(-) Enzyme	-0,034	-0,0034	-2,56E-07	-6,39E-05	-6,39E-01
(-) 1,2-Propanediol [S]	0,577	0,0577	4,34E-06	1,08E-03	1,08E+01
(-) B12 [S]	0,568	0,0568	4,27E-06	1,07E-03	1,07E+01